Molecular Microbiology (2015) ■ doi:10.1111/mmi.13021

Distinct contribution of *Toxoplasma gondii* rhomboid proteases 4 and 5 to micronemal protein protease 1 activity during invasion

George Rugarabamu,[1] Jean-Baptiste Marq,[1] Amandine Guérin,[2] Maryse Lebrun[2] and Dominique Soldati-Favre[1]*

[1]*Department of Microbiology and Molecular Medicine, CMU, University of Geneva, 1 Rue Michel-Servet, 1211 Geneva 4, Switzerland.*

[2]*UMR 5235 CNRS, Université de Montpellier 2, 34095 Montpellier, France.*

Summary

Host cell entry by the Apicomplexa is associated with the sequential secretion of invasion factors from specialized apical organelles. Secretion of micronemal proteins (MICs) complexes by *Toxoplasma gondii* facilitates parasite gliding motility, host cell attachment and entry, as well as egress from infected cells. The shedding of MICs during these steps is mediated by micronemal protein proteases MPP1, MPP2 and MPP3. The constitutive activity of MPP1 leads to the cleavage of transmembrane MICs and is linked to the surface rhomboid protease 4 (ROM4) and possibly to rhomboid protease 5 (ROM5). To determine their importance and respective contribution to MPP1 activity, in this study *ROM4* and *ROM5* genes were abrogated using Cre-recombinase and CRISPR-Cas9 nuclease, respectively, and shown to be dispensable for parasite survival. Parasites lacking ROM4 predominantly engage in twirling motility and exhibit enhanced attachment and impaired invasion, whereas intracellular growth and egress is not affected. The substrates MIC2 and MIC6 are not cleaved in *rom4-ko* parasites, in contrast, intramembrane cleavage of AMA1 is reduced but not completely abolished. Shedding of MICs and invasion are not altered in the absence of ROM5; however, this protease responsible for the residual cleavage of AMA1 is able to cleave other AMA family members and exhibits a detectable contribution to invasion in the absence of ROM4.

Accepted 31 March, 2015. *For correspondence. E-mail dominique.soldati-favre@unige.ch; Tel. (+41) 22 379 5672; Fax (+41) 22 379 5702.

© 2015 John Wiley & Sons Ltd

Introduction

The phylum Apicomplexa is comprised of a large and diverse group of obligate intracellular parasites that cause significant morbidity and mortality in both livestock and humans. Members of this phylum include *Toxoplasma gondii* and *Plasmodium falciparum*, the causative agents of toxoplasmosis and malaria respectively. Implicit in disease progression upon *T. gondii* infection is the asexual lytic cycle, which is initiated and subsequently progresses through multiple steps. These steps include egress from infected host cells, substrate-dependent gliding motility, attachment to host cells, reorientation to form a ring-like electron-dense moving junction (MJ) between the parasite and host cell membranes, host cell penetration, sealing of the parasitophorous vacuole membrane (PVM) and intracellular replication (Sibley, 2010). Within the parasitophorous vacuole (PV), *T. gondii* parasites divide by a specialized process termed endodyogeny, whereby daughter cells are formed within the mother cell after each round of DNA replication (Hu *et al.*, 2002).

Toxoplasma gondii uses the actomyosin system to power gliding motility, invasion and egress from infected cells. These processes are reliant upon synchronized and sequential secretion of a large repertoire of proteins from specialized apical organelles termed the micronemes and rhoptries (Carruthers and Sibley, 1997). Micronemal proteins (MICs) include transmembrane and soluble proteins that express different adhesive domains and assemble in complexes that are ultimately deposited onto the parasite surface (Sheiner *et al.*, 2010). These MICs redistribute over the entire parasite surface and interact with the host extracellular matrix to mediate gliding motility and with host cell receptors for attachment and penetration (Carruthers *et al.*, 1999). Specifically, the MIC2-M2AP complex is involved in gliding motility (Huynh *et al.*, 2003; Huynh and Carruthers, 2006), the MIC6-MIC1-MIC4 complex contributes to parasite attachment and invasion (Reiss *et al.*, 2001; Cerede *et al.*, 2005), the MIC8 complex is associ-

ated with rhoptry secretion (Kessler *et al.*, 2008) and the AMA1-RONs complex, which forms part of the MJ, is important for attachment and invasion (Mital *et al.*, 2005; Bargieri *et al.*, 2013; Lamarque *et al.*, 2014). The cytosolic domains (CTD) of MIC2, MIC6, MIC12 and AMA1 were thought to associate with the parasite actin cytoskeleton via an aldolase link (Jewett and Sibley, 2003; Sheiner *et al.*, 2010). However, more recently, the role of aldolase in mediating interactions of actin with AMA1 CTD has been revisited (Shen and Sibley, 2014) and whether aldolase is critical or not as connector for other MICs CTD such as MIC2 and MIC6, or if more plausibly another physiological connector exits, remain to be determined.

The efficiency of invasion requires the shedding of MICs by micronemal protein protease (MPP1, MPP2 and MPP3) activities (Zhou *et al.*, 2004). Although MPP2 and MPP3 cleave MIC2 ectodomain, as well as the soluble MICs such as M2AP, MIC4 and SUB1 (Carruthers *et al.*, 2000; Brecht *et al.*, 2001; Zhou *et al.*, 2004; Lagal *et al.*, 2010), MPP1 is involved in intramembrane cleavage of MIC2, MIC6, MIC12, AMA1 and MIC16 (Opitz *et al.*, 2002; Brossier *et al.*, 2003; Zhou *et al.*, 2004; Howell *et al.*, 2005; Buguliskis *et al.*, 2010; Sheiner *et al.*, 2010). Insertion of intramembrane cleavage mutations in MIC2 and AMA1 was reported to be deleterious to the parasite lytic cycle during the invasion step (Opitz *et al.*, 2002; Brossier *et al.*, 2003; Parussini *et al.*, 2012). Predicted contributors to MPP1 activity in *T. gondii* include the closely related rhomboids ROM4 and ROM5, both of which localize to the parasite surface and are conserved across the phylum (Brossier *et al.*, 2005; Dowse *et al.*, 2005; Buguliskis *et al.*, 2010; Sibley, 2013).

Previous work on ROM4 has highlighted a potential dual function during the *T. gondii* lytic cycle. Conditional knockdown of *ROM4* using a tetracycline repressible system (cko) led to the accumulation of AMA1 and MIC2 on the parasite surface, and caused a partial impairment in parasite invasion without impacting on intracellular growth (Buguliskis *et al.*, 2010). In contrast, the conditional stabilization of a catalytically inactive mutant form of this protease (ddROM4$_{S\text{-}A}$) severely blocked parasite replication without impacting on invasion (Santos *et al.*, 2011). When the cleavage product of AMA1 was coexpressed in the ddROM4$_{S\text{-}A}$ mutant, the block in intracellular growth was relieved (Santos *et al.*, 2011). These apparently contradictory observations on ROM4 function may be a result of the intrinsic limitations of the genetic systems used, and potentially due to a functional redundancy with ROM5.

To more conclusively dissect the contribution of ROM4 and ROM5 to MPP1 activity, we generated single and double knockouts using a combination of Cre-mediated excision in gene locus (Andenmatten *et al.*, 2013), as well as CRISPR-Cas9 nuclease-mediated gene disruption methodologies (Shen *et al.*, 2014a; Sidik *et al.*, 2014). The successful generation of clonal *ROM4* knockout (*rom4-ko*) strain demonstrates that this protease is dispensable for parasite survival. Although parasites lacking ROM4 are modestly impaired in their lytic cycle during the attachment-invasion step, we demonstrate that ROM4 contributes to the majority of MPP1 activity by cleaving AMA1, MIC2 and MIC6. We generated both *ROM5* knockdown (*rom5-kd*) and knockout (*rom5-ko*) by using the recently described methodologies in *T. gondii* for U1 small nuclear ribonucleic particle (snRNP)-mediated gene silencing (Pieperhoff *et al.*, 2014) and the CRISPR-Cas9 system respectively. Neither *rom5-kd* nor *rom5-ko* abrogated the shedding of endogenous transmembrane MICs, and absence of ROM5 had no impact on the parasite lytic cycle. Residual intramembrane processing of AMA1 is observed in *rom4-ko* strain, which is independent from stimulation of microneme secretion and is abolished to large extent in *rom4-ko/rom5-kd* and completely in *rom4-ko/rom5-ko* parasites. Importantly, in absence of ROM4, the contribution of ROM5 becomes evident as *rom4-ko/rom5-ko* parasites exhibit an aggravated invasion defect compared with *rom4-ko* parasites. MIC2 remains excluded from the surface of internalized *rom4-ko* and *rom4-ko/rom5-ko* parasites demonstrating that the capping phenomenon is not linked to MPP1 activity. Overall, this work highlights the predominant role of ROM4 in shedding MICs at the parasite surface and hence critically contributes to parasite reorientation consistent with another recent report (Shen *et al.*, 2014b). It also delineates a distinct role played by the closely related protease ROM5, which cleaves exclusively the AMA family members but in a restricted fashion due to limited substrate accessibility.

Results

Generation of ROM4 *null parasites by di-Cre mediated gene excision*

ROM4 was replaced with floxed *mycROM4* cDNA by double homologous recombination in the *ku80-ko* diCre-expressing strain (Fig. S1A) (Andenmatten *et al.*, 2013). This strategy also inserted a promoter-less YFP reporter just downstream of the *tubulin* promoter-driven *mycROM4* that would lead to YFP-expression upon diCre-mediated excision (Fig. S1A). The resulting strain (*rom4^{flox}*) was amenable to diCre-mediated *mycROM4* excision upon addition of rapamycin. Immunoblot analyses of resultant clonal *rom4^{flox}* parasites demonstrated migration of mycROM4 at the expected size of 72 kDa (Fig. 1A), and indirect immunofluorescence assays (IFA) displayed uniform mycROM4 localization across the parasite surface (Fig. 1B, top row). The correct integration of the floxed *mycROM4* at the endogenous *ROM4* locus was verified by

© 2015 John Wiley & Sons Ltd, *Molecular Microbiology*

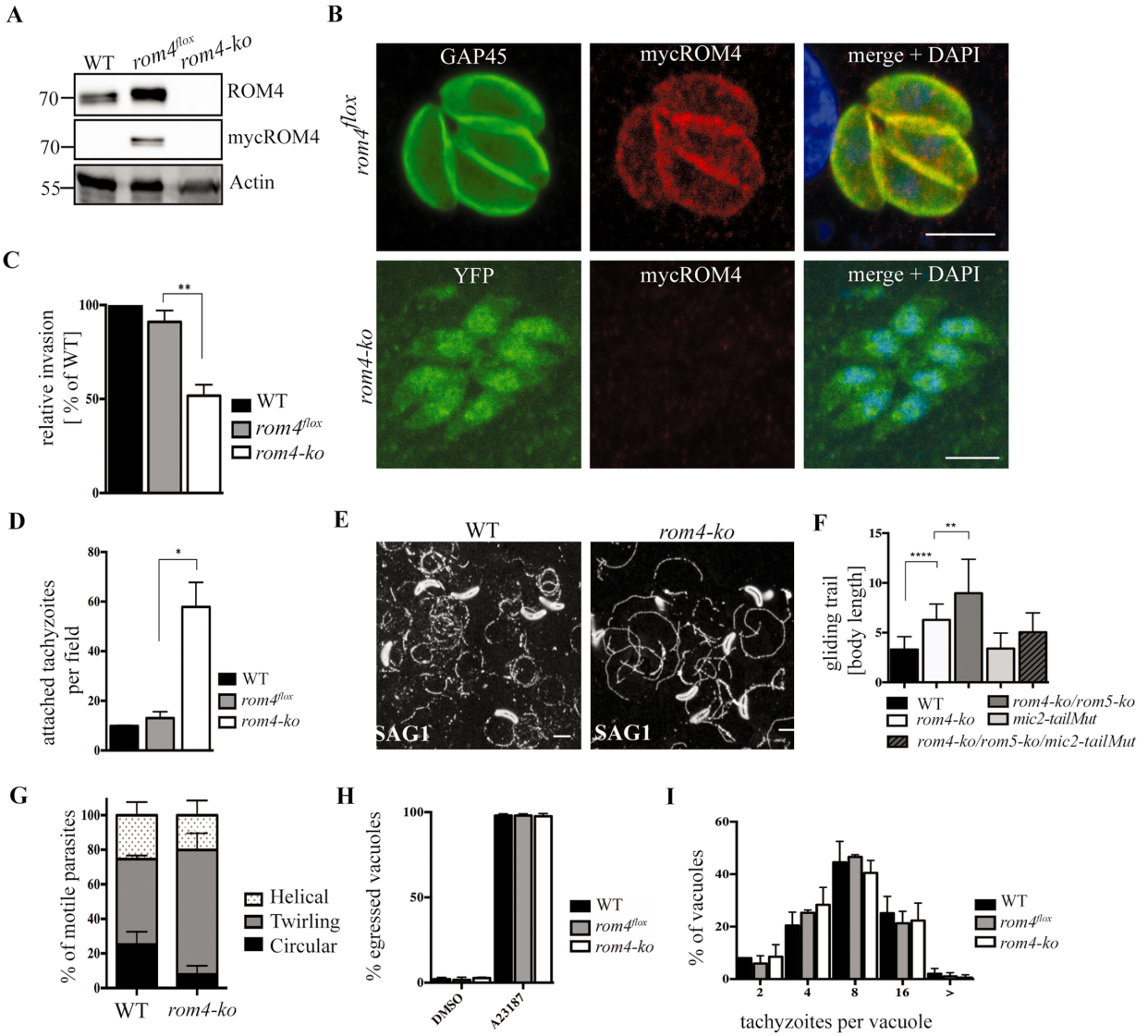


Fig. 1. Isolation and phenotypic analysis of *rom4-ko* parasites.
A. Immunoblot analyses indicating stable expression of mycROM4 in *rom4*^{flox} lysates and the absence of ROM4 in *rom4-ko* lysates. WT denotes *ku80::diCre*. Actin was used as loading control. Molecular weight is indicated in kDa.
B. Immunofluorescence analyses (IFA) depicting circumferential localization of mycROM4 on the surface of *rom4*^{flox} parasites (top row), and its absence in *rom4-ko* parasites that instead express YFP (bottom row). Green (top row), anti-GAP45 antibodies (Abs); green (bottom row), YFP; red, anti-myc monoclonal Abs; blue, DAPI. Scale bar, 5 μm.
C. Invasion assays reveal a modest impairment in invasion of *rom4-ko* parasites compared with parental strains. Data represents relative invasion (vs. *ku80::diCre*) of parasites successfully invading HFF monolayers within 30 min of inoculation, and comprise means ± standard deviation (SD) from at least 50 parasites counted in duplicate from three independent experiments. Statistical significance was determined by the Student's *t*-test (**$P < 0.005$).
D. *rom4-ko* parasites have an increased adhesion phenotype compared with parental strains. Adhesion to HFF monolayers was assessed by treating freshly egressed parasites with 1 μM Cytochalasin-D (CytD) to block motility and invasion, followed by inoculation on HFF monolayers for 15 min. Data represents mean ± SD from at least 50 parasites counted in duplicate from 3 independent experiments. Statistical significance was determined by the Student's t test ($P < 0.025$).
E. *rom4-ko* parasites undertake gliding motility as revealed by anti-SAG1 staining of trails deposited on FBS-coated cover slips.
F. Quantification of gliding trail length from various mutants represented relative to parasite body length (approximately 7 μm) (Barragan and Sibley, 2002). Data represents mean ± SD from 2 independent experiments. Statistical significance was determined by the Student's t test (**$P < 0.005$, ***$P < 0.0001$).
G. Quantification of gliding-motility-forms by live video-microscopy reveals predominant twirling gliding motility of *rom4-ko* parasites. Forms of gliding motility (circular, twirling, helical) among gliding parasites were analyzed from live-imaging video microscopy.
H. Parasites grown for 40 h were induced to egress by treatment with 3 μM calcium ionophore (A23187) for 7 min. The number of lysed vacuoles ($n = 100$) in DMSO vs. A23187 treatment was scored from 2 independent experiments.
I. Standard intracellular growth assays revealed that intracellular growth is not impaired in *rom4-ko* parasites. Data represents mean ± SD from at least 100 vacuoles counted from 3 independent experiments.

© 2015 John Wiley & Sons Ltd, *Molecular Microbiology*

PCR on genomic DNA (Fig. S1B–D). An average excision rate of ≈ 40% for *mycROM4* was achieved upon rapamycin induced activation of diCre in *rom4*^{flox} parasites (Fig. S1E). Parasite clones lacking *ROM4* were readily isolated as verified by genomic PCR (Fig. S1B–D), immunoblot analyses (Fig. 1A), and IFA (Fig. 1B, bottom row), demonstrating that *ROM4* is dispensable for parasite survival.

ROM4 *deletion leads to partial impairment in host-cell invasion*

A variety of assays designed to probe each specific step of the *ROM4* null parasites lytic cycle were conducted. Invasion assays were performed in which parasites were inoculated on human foreskin fibroblast (HFF) monolayers and invasion was monitored within a 30 min time-window. Although *rom4*^{flox} parasites maintained an invasion capability comparable with wild-type parasites (WT; *ku80-ko* diCre-expressing strain), *rom4-ko* parasites showed a ≈ 50% decrease in invasion efficiency relative to the WT control (Fig. 1C).

Host cell invasion by *T. gondii* encompasses multiple facets of host-parasite interaction and any of these steps may be compromised in the *rom4-ko* strain, accounting for the invasion phenotype observed here. Key among these steps is parasite attachment to the host cell monolayer. To test the contribution of ROM4 to this step, we blocked gliding motility and invasion in freshly egressed parasites by incubating them with Cytochalasin-D (CytD), an inhibitor of actin polymerization (Dobrowolski and Sibley, 1996), and subsequently incubating them on HFF monolayers for 15 min. Such treatment de-couples gliding motility and attachment in the invasion process, facilitating the study of attachment as a singular event. Subsequent assessment of *rom4-ko* parasite attachment showed a fourfold increase in adhesion when compared with WT parasites (Fig. 1D).

We next assayed the capability of *rom4-ko* parasites to glide on a substratum as various molecular factors involved in this process are also linked to host cell penetration. As *T. gondii* parasites glide on a substrate, a trail rich in surface proteins including the GPI-anchored surface protein SAG1, as well as plasma membrane (PM) lipids are deposited at the rear of the parasite and can be visualized by IFA (Dobrowolski and Sibley, 1996; Hakansson *et al*., 1999). SAG1 trails were observed in both *rom4-ko* and WT parasites during gliding assays on fetal bovine serum (FBS)-coated coverslips, with the former showing significantly longer trails (Fig. 1E and F). *T. gondii* parasites exhibit three distinct modes of gliding motion, namely circular and helical that generate a net positive movement, and twirling motility during which parasites appear upright with their posterior-end juxtaposed to the surface while their anterior portion repeatedly twirls (Frixione *et al*., 1996; Hakansson *et al*., 1999). To dissect these forms of gliding motion and their dynamics in absence of *ROM4*, we utilized live video-microscopy of gliding parasites upon deposition on FBS-coated dishes or during induced egress from HFF monolayer. These analyses revealed that the majority of *rom4-ko* parasites glide predominantly in a twirling form, and the frequency of helical and circular gliding is reduced compared with WT (Fig. 1G). In addition, investigations into the ability of *rom4-ko* parasites to egress from infected cells upon stimulation with calcium ionophore (A23187) revealed no defect (Fig. 1H). However, after completion of egress, *rom4-ko* parasites showed a considerably prolonged adhesion to the ruptured extracellular substratum and twirled repeatedly prior to engaging in other forms of gliding motion (compare Movie S1 and Movie S2 to Movie S3 and Movie S4). Altogether, these results indicate that *rom4-ko* parasites display a prolonged adhesion phenotype that impairs gliding motility and impedes invasion.

Following host cell penetration, *T. gondii* establishes its niche within the PV and initiates multiple rounds of cell division. Despite the previous reported block in intracellular growth induced by a ddROM4$_{S\text{-}A}$ catalytic mutant *rom4-ko* parasites showed no defect in intracellular growth (Fig. 1I).

ROM4 contributes to a substantial proportion of MPP1 activity

Upon apical release MICs rapidly redistribute on the parasite surface, accumulate at the rear and are eventually shed by MPP-based enzymatic activities that disengage host receptor-ligand interactions (Dowse and Soldati, 2004; Sibley, 2013).

As the processing pattern of various MICs found in excretory secreted antigens (ESA) as detected by immunoblot is known (Carruthers *et al*., 2000; Donahue *et al*., 2000; Brecht *et al*., 2001; Meissner *et al*., 2002; Opitz *et al*., 2002), we directly assessed the impact of *ROM4* deletion on the cleavage products of MPP1-based activity. Freshly egressed *rom4-ko* and WT parasites were stimulated to secrete MICs and subsequent immunoblot analyses of ESA fractions revealed equivalent levels of the dense granule protein GRA1 in both strains indicating comparable parasite viability (Sibley *et al*., 1995) (Fig. 2A). MIC4 (72 kDa), a soluble MIC part of the MIC1-4-6 complex, is processed upon microneme secretion in its N-terminus by MPP3 releasing the 70 kDa fragment that is thereafter processed by MPP2 in the C-terminus to release the 50 and 15 kDa fragments and thus abrogating its interaction with the MIC1-MIC6 complex (Brecht *et al*., 2001; Zhou *et al*., 2004). We used MIC4 as control of MICs without a transmembrane domain (TMD), and as such it underwent MPP2- and MPP3-based processing releasing

© 2015 John Wiley & Sons Ltd, *Molecular Microbiology*

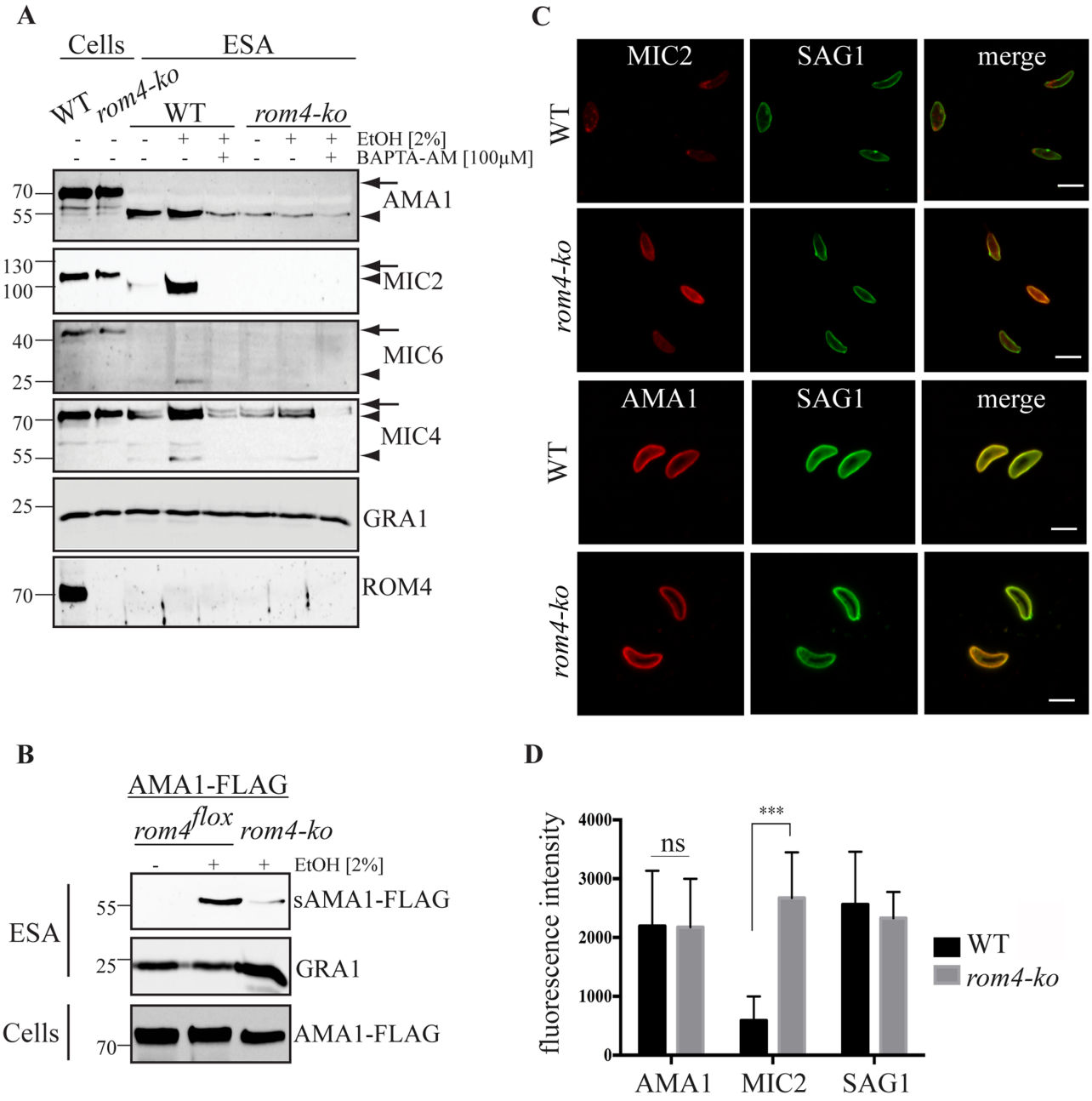


Fig. 2. Transmembrane MICs accumulate on *rom4-ko* parasite surface.
A. Immunoblot analyses of ESA from *rom4-ko* and WT (*ku80::diCre*) parasites upon stimulation with 2% Ethanol (EtOH) show impaired cleavage of the transmembrane MICs; AMA1, MIC2 and MIC6. Pretreatment with BAPTA-AM blocks MIC2, MIC4 and MIC6 secretion in WT and *rom4-ko* parasites but does not completely ablate AMA1 secretion. Denoted throughout are full-length (arrow) and shed fragments (arrowhead). GRA1 was included as a loading control and marker of parasite viability. MIC4, part of the MIC1-4-6 complex, was included as a soluble MICs control. Molecular weight is indicated in kDa.
B. Expression of an additional copy of N-terminal FLAG-tagged AMA1 confirms the residual shedding of AMA1 in *rom4-ko* parasites as seen in the ESA fraction labeled with anti-FLAG Abs (sAMA1-FLAG). Molecular weight is indicated in kDa.
C. IFA of extracellular parasites stimulated with 2% EtOH to enhance secretion of MICs reveals strong accumulation of MIC2 (top panels) but not AMA1 (bottom panels) on the *rom4-ko* parasite surface. Red, AMA1 and MIC2 were labeled using respective Abs directed against their ectodomain; green, anti-SAG1 mAbs. Scale bar, 5 µm.
D. Quantification of fluorescence intensity from IFAs in (C). Data represents mean ± SD from two independent experiments. ***$P < 0.001$ by two-way ANOVA.

© 2015 John Wiley & Sons Ltd, *Molecular Microbiology*

50 and 70 kDa fragments both in WT and *rom4-ko* parasites (Fig. 2A), albeit inefficiently so for the latter possibly due to the abrogated processing of MIC6 from the MIC1-4-6 complex (see below, and Fig. S4D). In contrast, the intramembrane processing products of MICs such as MIC2 (95 kDa) and MIC6 (35 kDa) were absent from the *rom4-ko* ESA, indicating impairment in MPP1 activity (Fig. 2A). However, among the transmembrane MICs, a faint 53 kDa AMA1 fragment could still be detected in the *rom4-ko* ESA (Fig. 2A) using anti-AMA1$_{folded}$ ectodomain I, II, III antibodies (Lamarque *et al*., 2014). This residual shedding of AMA1 in *rom4-ko* parasites was independent of stimulation of microneme secretion and was not blocked by treatment with the intracellular calcium chelator BAPTA-AM (Fig. 2A). To rule out the possibility of a cross-reaction of the anti-AMA1 antibodies with an unrelated protein, the residual shedding of AMA1 in *rom4-ko* strain was confirmed by expressing an additional copy of FLAG-tagged AMA1 (Fig. 2B). This cleavage profile of FLAG-tagged AMA1 in *rom4-ko* was reminiscent of the endogenous AMA1 shedding in *rom4-ko* (Fig. 2A), confirming that the residual shedding of AMA1 in absence of ROM4 is indeed not an artifact.

As these results suggest a reduced shedding of transmembrane MICs in *rom4-ko* parasites, we tested if this was concomitantly associated with an increase in the surface expression of MICs. To this end, IFAs were performed on non-permeabilized extracellular parasites stimulated to secrete MICs. A significant accumulation of MIC2 was observed on the surface of *rom4-ko* parasites when, compared with WT, whereas no obvious difference was detectable for AMA1, a protein abundantly secreted on the surface of extracellular parasites (Fig. 2C and D).

To assess the repertoire of ROM4 transmembrane MICs substrates, equal amount of ESA were collected from both *rom4-ko* and WT parasites and analyzed by mass spectroscopy (MS). Supplementary table 1 report the peptides detected within the ESA via multidimensional protein identification technology analysis (MudPIT). Although the quantity of peptides from dense-granule proteins and some soluble MICs was detected in equivalent amounts in both WT and *rom4-ko* samples, the peptide abundance of transmembrane MICs in the ESA was shifted between the two samples, with the WT ESA containing more detected peptides mapping to the ectodomain of transmembrane MICs (Supplementary table 1). Consistent with data presented in Fig. 2A, the semi-quantitative MS of *rom4-ko* ESA suggested impaired processing of MIC2, AMA1 and MIC8 (Supplementary table 1). Interestingly, TGME49_294330, which also has a predicted TMD, was also differentially detected in the MudPIT data (Supplementary table 1). The N-terminus of TGME49_294330 contains 6-EGF-domains, as well as DI and DII domains of the AMA family and has recently been characterized as a microneme protein called AMA4 (Lamarque *et al*., 2014).

MIC2 does not traverse the moving junction in the absence of ROM4

The results from ESA analyses prompted us to subsequently assess the fate of transmembrane MICs upon natural shedding during host–cell penetration. With the exception of AMA1 (Howell *et al*., 2005), capping of MICs is normally observed on the surface of WT parasites during host cell invasion, excluding them from the forming PV (Carruthers and Sibley, 1997; Carruthers *et al*., 2000; Garcia-Reguet *et al*., 2000; Howell *et al*., 2005; Brydges *et al*., 2006). Invasion was synchronized by allowing parasites to settle on HFF monolayers in non-permissive conditions prior to switching to invasion permissive conditions for 2 min (Lebrun *et al*., 2005). As previously described (Howell *et al*., 2005), the AMA1 ectodomain was detected on the internalized portion of the parasite surface in WT, as well as in *rom4-ko* parasites by IFA (Fig. 3A). Similarly to WT parasites, we could not detect MIC2 on the internalized surface of *rom4-ko* parasites (Fig. 3A, bottom 3 rows). However, we instead detected a dense 'dot' of MIC2 adjacent to fully invaded *rom4-ko* parasites, which was never observed in WT parasites (Fig. 3A). There was no similar accumulation of AMA1 dot in fully invaded *rom4-ko* parasites (data not shown). Further quantification revealed that the MIC2 dot was observed in a wide distribution averaging 1.5 μm (± 0.93, $n = 74$) from the PVM during the 2 min pulse invasion assays, which tends to suggest that the dot is detached not only from the parasite but also from the PVM (Fig. 3A and B). These results indicate that during invasion MIC2 is excluded from the forming PV in a ROM4-independent manner, and are in agreement with observations from a recent study on *Toxoplasma* rhomboids (Shen *et al*., 2014b).

As a consequence uncleaved MIC2 was detected upon western blot of culture supernatants from HFF monolayers infected (60 min) with *rom4-ko* but not with WT parasites (Fig. 3C). The corresponding intramembrane cleavage products of MIC2 (95–100 kDa) were only detected in the supernatant from WT parasites (Fig. 3C). In contrast, the AMA1 cleavage product (53 kDa) was detected in supernatants from *rom4-ko* parasite, although in less amount compared with the WT control (Fig. 3C). In this assay, the 70 kDa and 50 kDa fragments from MPP2 and MPP3 cleavage of MIC4 were detected in both WT and *rom4-ko* supernatants, implying complete shedding of MIC4 from the MIC1-MIC6 complex during 60 min invasion conditions (Fig. 3C). Taken together our observations on intramembrane shedding during invasion demonstrate that once deposited on the parasite surface, MIC2 fails to be cleaved in the absence of ROM4, whereas AMA1 cleavage is

© 2015 John Wiley & Sons Ltd, *Molecular Microbiology*

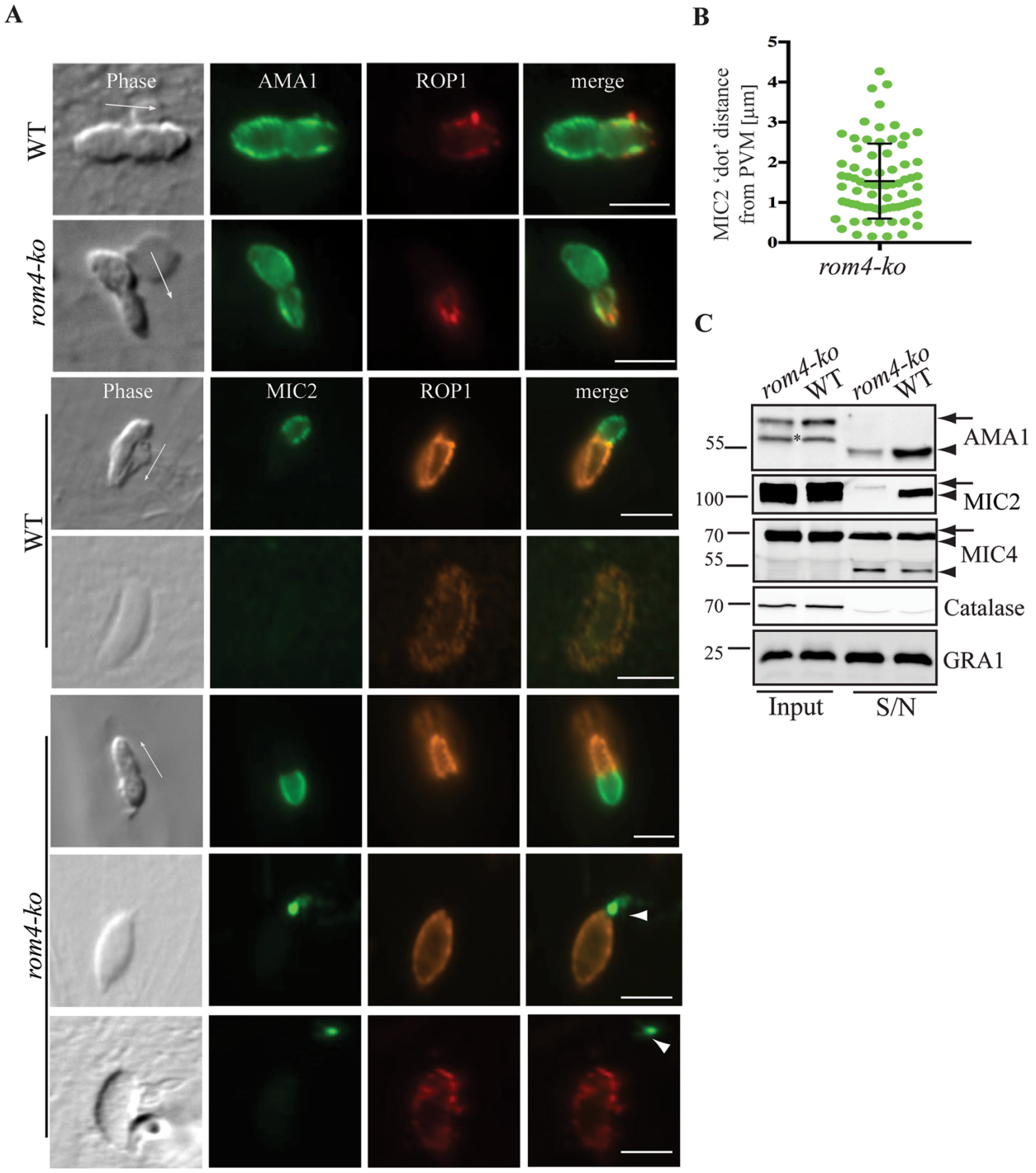


Fig. 3. Intramembrane cleavage of MIC2 is abrogated during invasion by *rom4-ko* parasites.
A. IFA of invading parasites treated with 0.1% saponin to permeabilize host cell PM and PVM but not parasite PM reveals AMA1 traversal through the moving junction (MJ) in *rom4-ko* parasites, whereas MIC2 is excluded. Green, AMA1 and MIC2 were labeled using Abs directed against their ectodomain; red, Anti-ROP1 Abs was used as a marker of the PV. Arrowhead indicates a prominent MIC2 dot adjacent to a sealing PV as detected by anti-MIC2 Abs. All images are single focal plane acquisition. Scale bar, 5 µm.
B. distribution plot of measured MIC2 dot distance from the PVM in fully invaded *rom4-ko* parasites during 2 min pulse-invasion assays. An average distance of 1.5 µm ± 0.94 ($n = 74$) was measured.
C. Immunoblot analyses of concentrated supernatant collected from culture medium upon inoculation of HFF monolayers with WT or *rom4-ko* parasites for 60 min. A residual intramembrane shedding product of AMA1 is detected in the supernatant (S/N) from *rom4-ko* parasite cultures, whereas that of MIC2 is not detected, instead an uncleaved MIC2 fragment is detected in *rom4-ko* S/N. Catalase was used as control for parasite lysis. Arrow; full-length protein. Arrowhead; shed fragment. Asterisks indicate the non-reduced form of full-length AMA1. Molecular weight is indicated in kDa.

© 2015 John Wiley & Sons Ltd, *Molecular Microbiology*

reduced but not completely abolished under these same conditions.

ROM5 is dispensable for parasite survival

Given that the residual shed AMA1 fragment observed in *rom4-ko* parasites corresponds to the molecular weight expected upon rhomboid protease cleavage, we turned our attention to the potential involvement of another closely related rhomboid protease, ROM5. IFA analyses of endogenously C-terminally tagged ROM5-3Ty in intracellular parasites revealed a peripheral localization with prominent accumulation at the posterior confirming previously published data on additional copy N-terminally tagged ROM5 (Fig. 4A, top row) (Brossier *et al*., 2005; Dowse *et al*., 2005). To investigate the precise localization of ROM5 which has a predicted topology similar to ROM4 (Sheiner *et al*., 2008), we examined non-permeabilized parasites and determined that ROM5-3Ty is barely detectable under such conditions (Fig. 4A, middle row). Conversely, upon permeabilization with 0.1% Triton X-100, ROM5-3Ty was readily detectable indicating that the majority of ROM5-3Ty is not present on the surface of the parasite and instead resides internal to this outer membrane (Fig. 4A, bottom row). Endogenous ROM5 was also tagged by a Myc epitope at its N-terminus using the newly *T. gondii*-adapted CRISPR-Cas9 based strategy (Fig. S3A) (Shen *et al*., 2014a; Sidik *et al*., 2014). Although we were able to confirm integration of the Myc epitope coding sequence (CDS) at the start of the *ROM5* and its detection by western blot (Fig. S3B–D), immunofluorescence analysis was not conclusive due to a weak signal (not shown). However, expression of N-terminus Myc-tagged ROM5 (mycROM5) under a strong promoter also confirmed previous IFA observations and was thus used in complementation experiments below (Fig. S3E) (Dowse *et al*., 2005). Nevertheless, tagging endogenous ROM5 at the C-terminus did not impair its activity (see below); therefore, this strain (*rom5-3ty*) was used for further analysis.

ROM5 has previously been shown to cleave a variety of MICs including *P. falciparum* AMA1 in cell-based assays (Brossier *et al*., 2005; Dowse *et al*., 2005; Baker *et al*., 2006); therefore, we investigated its contribution to MICs cleavage through both knockdown and knockout approaches. Knockdown of *ROM5* was achieved using the U1-snRNP-mediated gene silencing methodology recently adapted to *T. gondii* (Pieperhoff *et al*., 2014). This method involved appending U1 snRNP recognition sequences just downstream of the terminal exon to prevent alternative polyadenylation, thus leading to highly efficient mRNA decay and gene silencing (Gunderson *et al*., 1998; Fortes *et al*., 2003). This methodology combined with Cre-mediated positioning of U1 sequences downstream of the terminal exon of a gene-of-interest (GOI) has been successfully used in *T. gondii* to knockdown various genes (Pieperhoff *et al*., 2014).

Here we have introduced the pROM5-3ty-floxU1 plasmid into the *ROM5* locus by single-homologous recombination, inserting a floxed insert containing the *SAG1* 3′UTR, *HXGPRT* selection marker and four U1-snRNP recognition sequences downstream of *rom5-3ty* STOP codon (Fig. S2A). Cre-mediated excision subsequently positioned the U1 sequences just downstream of the *rom5-3ty* STOP codon mediating knockdown by degradation of *rom5-3ty* transcripts (Fig. S2A). We verified correct integration of the pROM5-3ty-floxU1 plasmid and Cre-mediated excision at the *ROM5* locus in WT and *rom4-ko* parasites by PCR amplification of genomic DNA (Fig. S2B). Following this methodology, we were able to readily isolate clonal parasites with reduced *rom5-3ty* expression (*rom5-kd* and *rom4-ko/rom5-kd*) (Fig. 4B and Fig. S2C).

To assess the functional impact of ROM5 depletion, we tested the ability of *rom5-kd* and *rom4-ko/rom5-kd* parasites to invade and grow intracellularly. In contrast to parental strains, *rom5-kd* parasites showed only a mild defect in invasion, whereas *rom4-ko/rom5-kd* parasites showed a slight but not significant additional reduction in invasion capability when compared with *rom4-ko*: ≈ 45% vs. 50% respectively (Fig. S4A). We observed no impact from silencing *ROM5* alone or in addition to *rom4-ko* during intracellular growth (Fig. S4B).

To rule out any contribution to MPP1 activity by residual ROM5 activity in *rom5-kd* parasites, the deletion of *ROM5* in parental *rom5-3ty* and *rom4-ko/rom5-3ty* strains was performed using the CRISPR-Cas9 based strategy (Shen *et al*., 2014a; Sidik *et al*., 2014). To induce a double strand break (DSB) at the *ROM5* loop 1 coding sequence, we co-transfected a cas9-gfp-ROM5gRNA expression plasmid together with a linear donor plasmid containing *ROM5* homology regions for DSB repair and replacement with a CAT cassette (Fig. S5A). Parental *rom4-ko* parasites transiently expressing cas9-gfp were sorted by FACS and cloned to generate *rom4-ko/rom5-ko* parasites, whereas *rom5-ko* parasites were readily obtained by conventional limiting dilution cloning (Fig. S5B). Genomic DNA PCR analysis confirmed the replacement of *ROM5* with a CAT selection cassette in both *rom5-ko* and *rom4-ko/rom5-ko* parasites (Fig. S5C). Western blot analyses revealed the absence of ROM5-3Ty in *rom5* knockout strains as well as the expression of mycROM5 in the complemented *rom4-ko/rom5-ko* strain (Fig. 4C). During growth competition assays *rom4-ko* parasite growth surpassed that of the *rom4-ko/rom5-ko* parasites by passage 3 (Fig. 4D), indicating reduced fitness of the latter. Phenotypic analyses of the *rom5-ko* strain confirmed our previous results that *ROM5* is dispensable for parasite survival (Fig. 4E–G). Intracellular growth was not impaired in *rom5-ko* or

© 2015 John Wiley & Sons Ltd, *Molecular Microbiology*

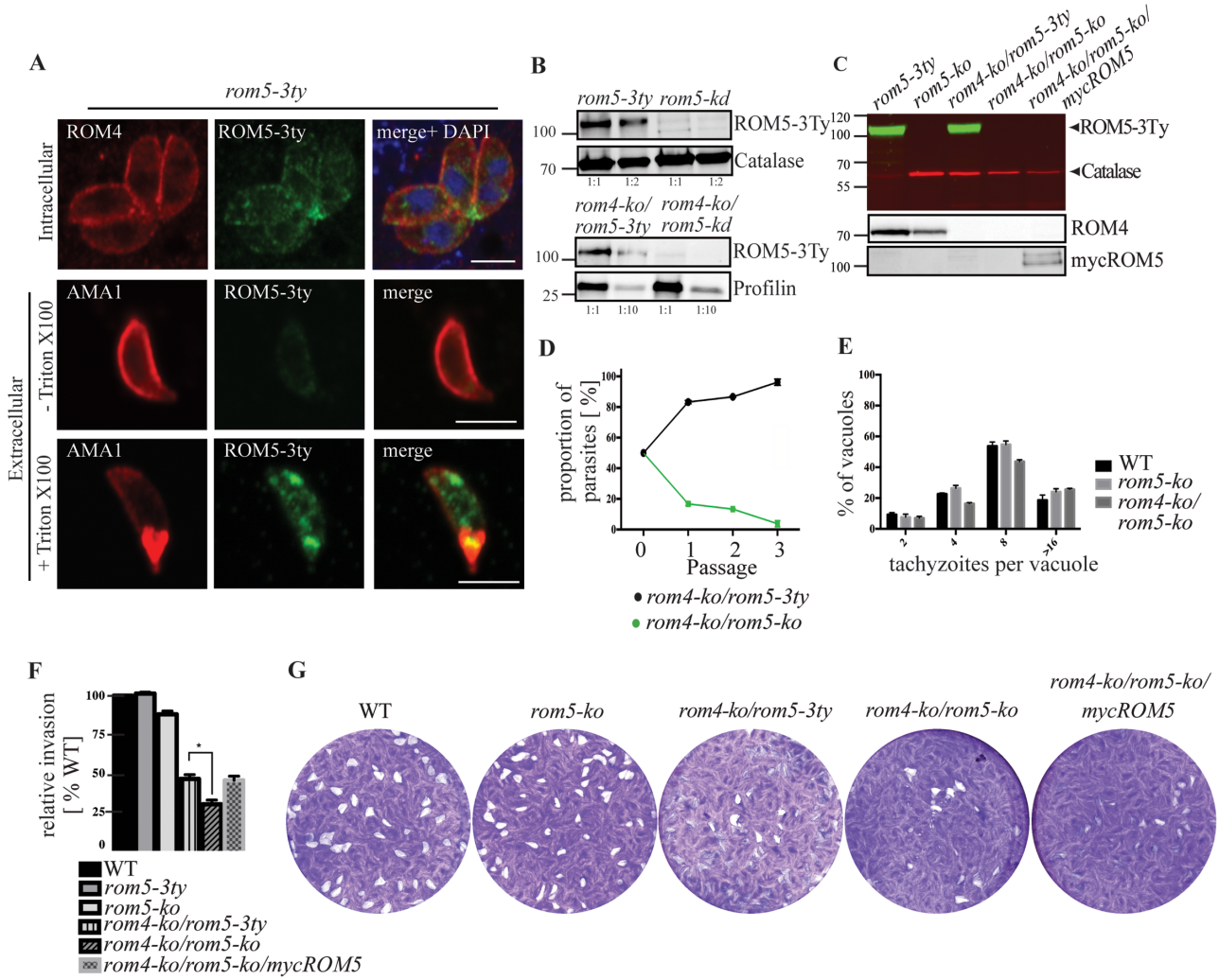


Fig. 4. Phenotypic characterization of *rom5-ko* parasites.
A. IFA using anti-Ty mAb demonstrates ROM5-3Ty localization to posterior vesicular structures in intracellular *rom5-3ty* parasites (top row). IFA of non-permeabilized extracellular parasites stimulated with 3 μM Ca^{2+} ionophore A23187 revealed minimal ROM5-3Ty on the parasite surface (middle row), whilst the majority is localized to intracellular vesicles as revealed upon permeabilization with 0.1% Triton X-100 (bottom row). Red, anti-AMA1 or anti-ROM4 Abs was used as a marker of the micronemes or parasite surface respectively; green, anti-Ty mAbs. Scale bar, 5 μm.
B. Western blot analyses of ROM5-3Ty expression and U1-snRNP mediated knockdown of *rom5-3ty* in WT (*ku80::diCre*) and *rom4* knockout background strains. Catalase and Profilin were used as loading controls. Shown are dilution series from protein extracts.
C. Western blot analyses of endogenous ROM5-3Ty expression and CRISPR-Cas9 mediated knockout in WT and *rom4* knockout background strains, as well as mycROM5 overexpression in the *rom4-ko/rom5-ko* strains. Catalase was used as a loading control. (B and C), molecular weight is indicated in kDa.
D. Growth competition assays show reduced fitness of *rom4-ko/rom5-ko* parasites compared with *rom4-ko/rom5-3ty* parental strain upon co-culture for three passages. Upon natural egress parasites were inoculated on HFF monolayers for 1 h before washing. The proportions of parasites growing after each passage (24 h) were determined by IFA with anti-Ty (*rom4-ko/rom5-3ty*) and anti-GAP45 Abs (total parasites). At least 100 vacuoles were counted from 2 independent experiments.
E. 24 h intracellular growth assays show no impairment in *rom5-ko* and *rom4-ko/rom5-ko* parasite growth. Data represents the mean ± SD from at least 100 vacuoles counted from three independent experiments.
F. Invasion assays revealed a drop in invasion of *rom4-ko/rom5-ko* parasites compared with parental strains. Data represent relative invasion (vs. *ku80::diCre*) of parasites successfully invading HFF monolayers within 30 min of inoculation, and comprise means ± SD counted from three independent experiments. Statistical significance was determined by the Student's *t*-test (**$P < 0.005$).
G. Plaque formation by parasites ($n = 50$) inoculated on HFF monolayers, incubated for 8 days at 37°C and stained with crystal violet show a slightly compromised plaque formation phenotypes for *rom4-ko* and *rom4-ko/rom5-ko* parasites.

© 2015 John Wiley & Sons Ltd, *Molecular Microbiology*

rom4-ko/rom5-ko parasites (Fig. 4E). Gliding motility as assessed by SAG1 trail deposition showed a similar trail pattern for *rom5-ko* and WT parasites; however, *rom4-ko/rom5-ko* parasites had considerably longer trails (Figs S8B and 1F). Although invasion analyses of *rom5-ko* parasites did not show a significant impairment, *rom4-ko/rom5-ko* parasites exhibited an aggravated invasion phenotype compared to *rom4-ko* parasites, that showed similar levels of invasion as the *rom4-ko/rom5-ko* mutant complemented with mycROM5 (Fig. 4F). Concordantly, plaque assays showed a slightly reduced plaque size for *rom4-ko* and *rom4-ko/rom5-ko* parasites, whereas *rom5-ko* parasites formed comparable sized plaques to WT parasites (Fig. 4G). In addition, infection of CD1 mice ($n = 5$) with 50 WT, *rom4-ko*, *rom4-ko/rom5-kd* or *rom4-ko/rom5-ko* parasites caused equal lethality around day 8 indicating that the mutant strains retain full virulence (Fig. S6). Combined, these results indicate that the contribution of both ROM4 and ROM5 is important to mediate successful host-cell invasion, but both genes are dispensable for parasite survival.

ROM5 is responsible for the residual shedding of AMA1 in the rom4-ko strain

To assess the impact of C-terminus tagging of ROM5 on its activity, we compared the residual AMA1 shedding between *rom4-ko* strains expressing untagged ROM5 (*rom4-ko*) and that with a C-terminus tag at *ROM5* locus (*rom4-ko/rom5-3ty*). Analysis of ESA contents showed comparable AMA1 shedding in both *rom4-ko* and *rom4-ko/rom5-3ty* parasites, demonstrating that ROM5-3Ty is functionally comparable with endogenous ROM5 (Fig. S4C).

To determine the contribution of ROM5 on transmembrane MICs shedding, ESA contents from *rom5-kd* and *rom4-ko/rom5-kd*, as well as, *rom5-ko* and *rom4-ko/rom5-ko* parasites were analyzed. Abrogating *ROM5* alone did not impact the shedding of AMA1, MIC2 or MIC6, implying that ROM5 does not contribute to a substantial proportion of MPP1 activity upon induced microneme secretion (Figs 5A and S4D). Importantly, however, the residual shedding of AMA1 seen in *rom4-ko* parasites was abolished in *rom4-ko/rom5-ko* parasites but was restored in the *rom4-ko/rom5-ko/mycROM5* complemented strain (Fig. 5A), indicating that ROM5 processes a subset of AMA1. The surface localization of AMA1 during invasion was not perturbed in either *rom5-kd* or *rom4-ko/rom5-kd* parasites, and in both cases AMA1 traversed the MJ without any apparent accumulation in the area of the invading parasite (Fig. 5B), similar to observations in WT and *rom4-ko* parasites. These results suggest that uncleaved AMA1 is not excluded from the surface of invading parasites and traverses the MJ. As observed in *rom4-ko* parasites, IFAs of invading parasites probed for the MIC2-ectodomain showed normal posterior capping in *rom5-kd* as well as in *rom4-ko/rom5-kd* parasites (Fig. 5B). The 'dot' of MIC2 staining observed adjacent to fully invaded *rom4-ko* parasites (Fig. 3A) was not detected in invaded *rom5-kd* parasites but was observed in *rom4-ko/rom5-kd* and *rom4-ko/rom5-ko* parasites using both anti-MIC2 ectodomain and anti-MIC2 tail antibodies respectively (Fig. 5B).

Collectively, these results reveal that: AMA1 is shed by ROM4 upon induction of microneme secretion, and also by ROM5 in a constitutive but limited manner. In addition, MIC2 and MIC6 are processed by ROM4 only, and the exclusion of MIC2 from the PV during invasion is mediated by a mechanism independent of its intramembrane cleavage.

AMA family members are cleaved by ROM4 and ROM5

Given our findings that both ROM4 and ROM5 contributed to the intramembrane cleavage of AMA1, we sought to investigate their contribution to the cleavage of other members of the AMA protein family. However, in contrast to AMA1, the remainder of AMA protein family members are weakly or not at all detectable in wild-type parasites (Poukchanski *et al*., 2013; Lamarque *et al*., 2014). To determine if AMA proteins are generally substrates for ROM5, we took advantage of a previously described method of assessing intramembrane proteolysis within parasites using N-terminal SAG1-Ty fusions bound to a variety of MICs transmembrane (TM) and cytosolic domains (SAG1-Ty-TM-CTD) (Fig. 6A and B) (Di Cristina *et al*., 2000; Reiss *et al*., 2001; Opitz *et al*., 2002; Sheiner *et al*., 2010). These SAG1-Ty-TM-CTD constructs are targeted directly to the micronemes when fused to escorter MICs CTD (MIC2 and MIC6), whereas MICs lacking trafficking signals in their CTD (AMA1) are routed likely via the dense granules in the constitutive secretion pathway (Di Cristina *et al*., 2000; Reiss *et al*., 2001; Opitz *et al*., 2002; Sheiner *et al*., 2010). When trafficked to the PM, these fusion-proteins are processed by MPP1 activity, and therefore, we have utilized this system to characterize the repertoire of transmembrane MICs shed in parasite strains lacking ROM4, ROM5 or both, as well as to assign protease-substrate pairs where possible.

Constructs containing the TM-CTD from AMA family members and other previously characterized transmembrane MICs were transiently transfected in WT, *rom4-ko*, *rom5-ko* and *rom4-ko/rom5-kd* or *rom4-ko/rom5-ko* strains. AMA family member SAG1-fusions were localized to the dense granules and vesicles along the secretory pathway in WT parasites and accumulated at the PM in *rom4-ko/rom5-ko* parasites (Fig. S7A). Western blot analysis of shed products from intracellular parasites revealed that both AMA1 and AMA2 fusions were cleaved in

© 2015 John Wiley & Sons Ltd, *Molecular Microbiology*

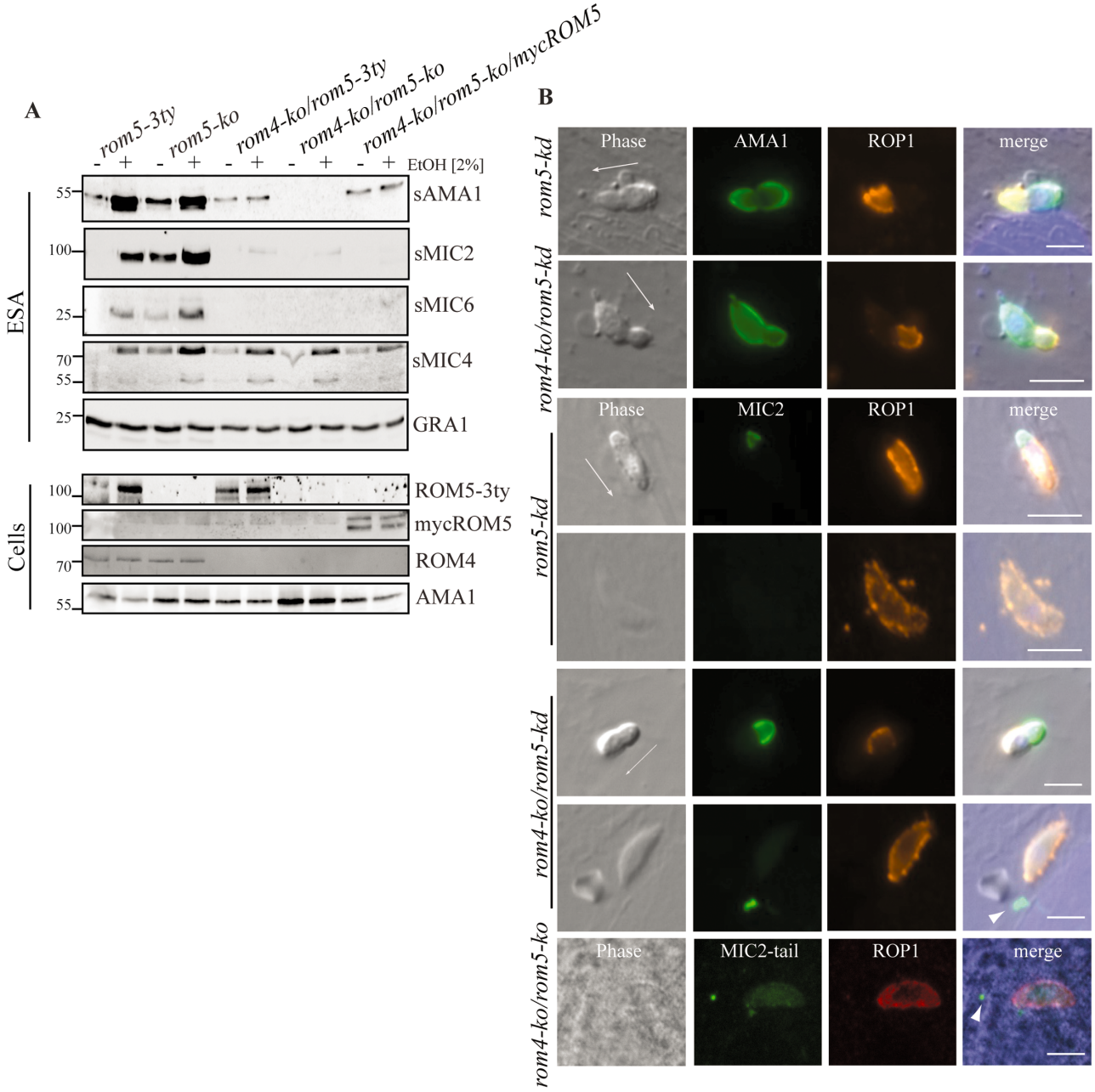


Fig. 5. ROM5 is responsible for residual AMA1 shedding in *rom4-ko* parasites.
A. Immunoblot analyses of ESA from *rom5-ko* parasites revealed wild-type levels of shed (s-) AMA1, MIC2 and MIC6. AMA1 shedding is abrogated in the *rom4-ko/rom5-ko* strain, while the residual AMA1 shedding was restored in the mycROM5 overexpressing strain *rom4-ko/rom5-ko/mycROM5*. GRA1 was included as a loading control and as marker of parasite viability. Molecular weight is indicated in kDa.
B. IFA of invading parasites treated with 0.1% saponin reveals MIC2 capping in *rom5-kd*, *rom4-ko/rom5-kd* and *rom4-ko/rom5-ko* parasites. Arrows denote direction of penetration and arrowhead indicates a prominent MIC2 'dot' adjacent to fully invaded *rom4-ko/rom5-kd* and *rom4-ko/rom5-ko* parasites as detected by anti-MIC2-ectodomain and anti-MIC2-tail Abs respectively (green). Red, Anti-ROP1 Abs were used as a marker of the PV. All images are single focal plane acquisition. Scale bar, 5 μm.

rom4-ko parasites, however cleavage was abolished in *rom5-ko* and *rom4-ko/rom5-ko* parasites (Fig. 6B), indicating that they are primarily processed by ROM5 during the constitutive secretion pathway. In contrast, AMA4 fusion was sensitive to combined abolition of both ROM4 and ROM5 (Fig. 6B). Notably, the cleavage of AMA2 and AMA4 was still detectable in the *rom4-ko/rom5-kd* parasites (Fig. S7C), indicating that even a small amount of ROM5 is still capable of mediating cleavage of AMA family members. In the case of MIC2, IFA data showed a proportion were mislocalized due to transient over-expression and accumulated at the parasite surface in *rom4-ko* parasites,

© 2015 John Wiley & Sons Ltd, *Molecular Microbiology*

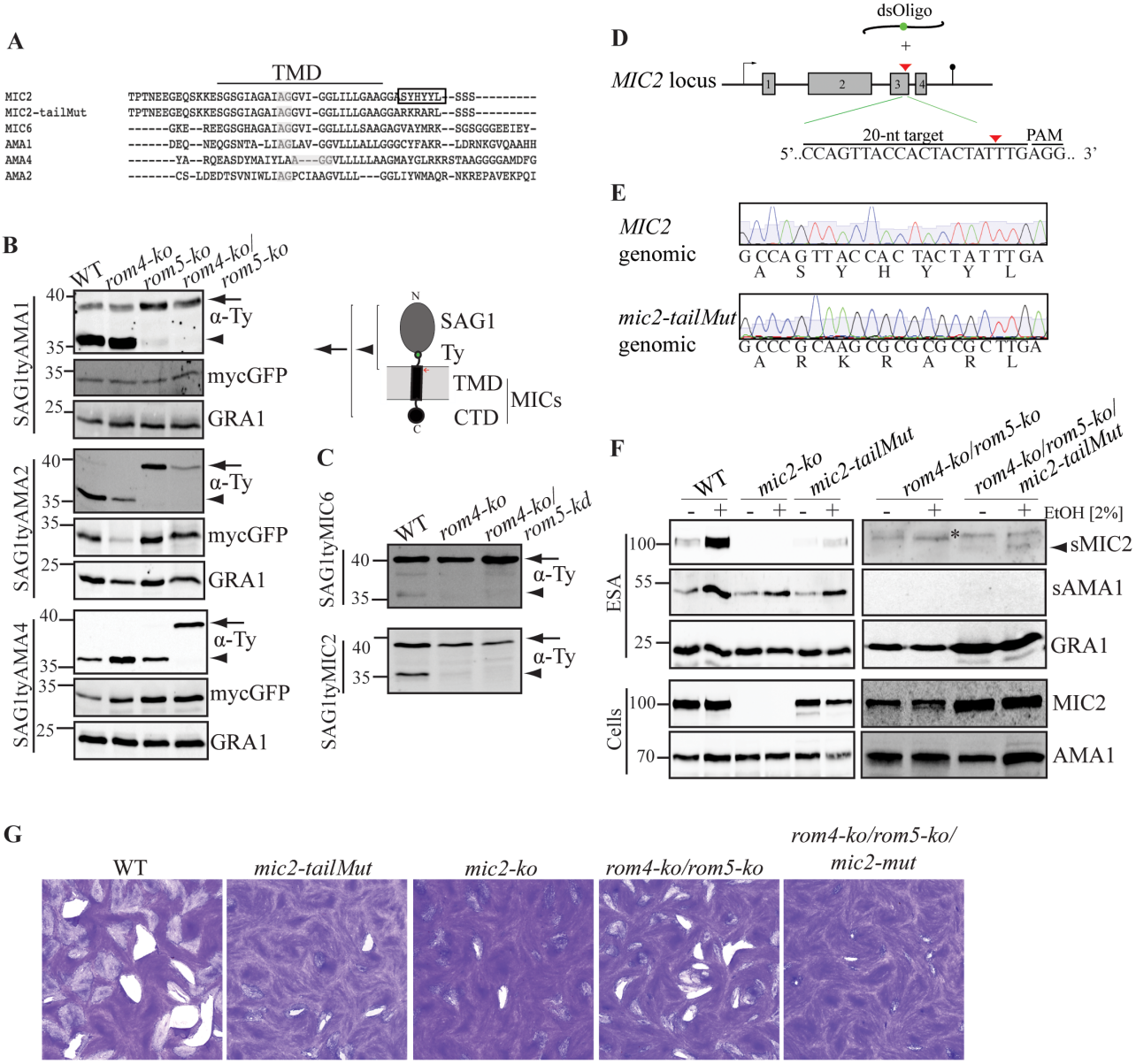


Fig. 6. Cleavage analysis of SAG1-Ty-TM-CTD chimera and mistargeted endogenous MIC2.

A. Sequence alignment of transmembrane domain (TMD) of various MICs. Highlighted are residues conducive for rhomboid proteolysis. Box: MIC2 cytoplasmic tail motif ^{721}SYHYY responsible for microneme targeting (Di Cristina *et al.*, 2000). (B and C, inset), schematic representation of the SAG1-Ty-TM-CTD chimera used for cleavage analysis.

B. Immunoblot analyses of the SAG1-Ty-AMA secretome from WT, *rom4-ko*, *rom5-ko* and *rom4-ko/rom5-ko* strains reveal residual shedding of AMA family members in *rom4-ko* parasites, which is abolished in *rom4-ko/rom5-ko* parasites. Arrows indicate mature proteins and arrowhead denotes shed products, both of which are detected with anti-Ty mAb. mycGFP was coexpressed as an internal control and was detected by anti-Myc Abs. GRA1 was included as a total loading control.

C. Immunoblot analyses of SAG1tyMIC2 and -MIC6 secretome from WT, *rom4-ko*, and *rom4-ko/rom5-kd* strains show the absence of shedding in *rom4-ko* parasite samples. Arrows indicate mature proteins and arrowhead denotes shed products both of which are detected with the anti-Ty mAb. (B and C), molecular weight is indicated in kDa.

D. Schematic of guide-RNA targeting strategy to induce DSB (red triangle) by Cas9 nuclease at the *MIC2* locus exon 3, and subsequent repair by 100 bp dsOligo that contains the microneme targeting motif mutation (^{721}SYHYY>RKRAR – *mic2-tailMut*) (Di Cristina *et al.*, 2000).

E. Sanger sequencing confirms introduction of *mic2-tailMut* at the *MIC2* locus.

F. *mic2-tailMut* is impaired in microneme secretion whereas residual MIC2 shedding is detected in *rom4-ko/rom5-ko/mic2-tailMut*. Arrowhead indicates the shed (s-) fragment of MIC2. Asterisks indicate full-length MIC2 inadvertently released in ESA. Molecular weight is indicated in kDa.

G. *rom4-ko/rom5-ko/mic2-tailMut* is impaired in plaque formation when compared with parental strain, whereas *mic2-ko* and *mic2-tailMut* showed a comparable reduced fitness.

© 2015 John Wiley & Sons Ltd, *Molecular Microbiology*

although most are in the micronemes as previously reported (Opitz *et al*., 2002) (Fig. S7B). As expected, MIC2 and MIC6 SAG1-fusions were not processed when expressed in *rom4-ko* parasites (Fig. 6C). These results demonstrate that ROM5 is a constitutively active rhomboid protease that cleaves TMD of AMA1 family members, but is inert toward those of MIC2 and MIC6.

It has been shown that endogenous MIC2 CTD contains a tyrosine-rich motif ^{721}SYHYY that contribute to its microneme targeting that is also preserved in the SAG1-ty-MIC2 construct (Di Cristina *et al*., 2000; Reiss *et al*., 2001; Sheiner *et al*., 2010). Therefore, to conclusively rule out that endogenous MIC2 could serve as substrate for ROM5 if rerouted to the default secretory pathway, we introduced mutations into the microneme-targeting motif of endogenous MIC2 (^{721}SYHYY-RKRAR, *mic2-tailMut*) using the CRISPR-Cas9 system in WT and *rom4-ko/rom5-ko* parasites (Fig. 6D and E). IFA showed the absence of MIC2 in the micronemes of *mic2-tailMut* strains but was instead mislocalized to vesicles in the secretory pathway (Fig. S8A). Using WT and *mic2-ko* parasites obtained by Cas9-nuclease as controls, analyses of ESA by western blot revealed that the MIC2-tailMut in WT background was largely uncleaved, whereas in *rom4-ko* (data not shown) but also in *rom4-ko/rom5-ko* backgrounds, residual cleavage could be detected (Fig. 6F). These results indicate that MIC2-tailMut routing via the constitutive pathway is not a substrate for ROM5 but is processed in this context by another rhomboid protease.

Phenotypically, *rom4-ko/rom5-ko/mic2-tailMut* parasites had a reduced gliding trail length compared with *rom4-ko/rom5-ko* parasites (Figs S8B and 1F). In addition, a comparative plaque assay analysis of *mic2-tailMut* and *rom4-ko/rom5-ko/mic2-tailMut* parasites revealed a fitness defect in the latter confirming that MIC2 is not only involved in parasite reorientation but also participates in additional steps of the lytic cycle (Fig. 6G). In this context it is relevant to note that *mic2-tailMut* and *mic2-ko* parasites exhibit comparable loss of fitness as detected by plaque assay (Fig. 6G).

Collectively, these results highlight a distinct substrate selectivity of and accessibility to ROM5 for AMA family members but not for MIC2.

Discussion

Proposed roles of intramembrane proteolysis of surface adhesins (MPP1-based activity) during the *T. gondii* lytic cycle include: disengaging parasite-host receptor-ligand interactions to facilitate gliding motility and host cell penetration, creating a gradient of adhesins to allow reorientation prior to penetration, and detachment of the parasite posterior from the newly sealed PVM at the end of the entry process. MPP1 activity has been associated with intramembrane cleavage of diverse transmembrane MICs and initial characterization of rhomboid proteases in *T. gondii* pointed toward ROM4 and ROM5 as primary candidates (Brossier *et al*., 2005; Dowse *et al*., 2005). More recently, the conditional knockdown of *ROM4* established that this protease contributes to MPP1 activity (Buguliskis *et al*., 2010), whereas a ROM4 catalytic inactive mutant (ddROM4$_{S\text{-}A}$) was reported to block intracellular replication without impacting invasion, an event rescued upon coexpression with the AMA1-tail (Santos *et al*., 2011). As invasion was not affected in ddROM4$_{S\text{-}A}$ expression studies, it was hypothesized that the presence of endogenous ROM4 precludes complete sequestration of invasion ligands normally shed during the invasion step. Also, in the case of the *rom4-cko* the absence of a defect in intracellular growth may be due to the observed (≈ 15%) residual expression of *rom4* (Buguliskis *et al*., 2010), which may be enough to trigger an intracellular growth signaling function by ROM4.

The implication of ROM4 and AMA1 as a signaling cascade leading to the switch from invasive to the replicative mode has been first challenged by the absence of replication defect in parasites expressing an uncleavable form of AMA1 (Parussini *et al*., 2012) or completely lacking AMA1 (Bargieri *et al*., 2013). The work presented here establishes the dispensability of both *ROM4* and *ROM5* for replication, thus confronting again the signaling model. In addition, a recent study presents a compelling biological analysis of the dispensability of *ROM1*, *ROM4* and *ROM5* alone, or together in all combinations, for parasite survival (Shen *et al*., 2014b). Whether the defect in intracellular growth observed by ddROM4$_{S\text{-}A}$ is due to cellular stress induced by the expression system or as a result of a sequestered substrate(s) remains to be clarified.

Analysis of the lytic cycle of mutant parasites in this study has revealed a significant contribution of ROM4 activity to the invasion step, consistent with recent reports (Buguliskis *et al*., 2010; Shen *et al*., 2014b). Freshly egressed *rom4-ko* parasites exhibited enhanced twirling motility, which is likely the result of MICs adhesins accumulating onto the parasite surface and being deposited toward the parasite posterior. The persistence of MICs on the parasite surface affected a fourfold increase in attachment to HFF monolayers when invasion was blocked by addition of CytD. This observation is consistent with the previous report showing increased adhesion to substratum by parasites expressing an uncleavable form of MIC2, as well as in *rom4-cko* parasites (Brossier *et al*., 2003; Buguliskis *et al*., 2010). Taken together the phenotypic consequences of *ROM4* deletion points toward a role in parasite reorientation only as *rom4-ko* parasites glide normally on substrate, are not arrested in the final step of the entry process, and replicate like WT parasites. Furthermore and importantly, the exclusion of MIC2 from

© 2015 John Wiley & Sons Ltd, *Molecular Microbiology*

the surface of invading parasites is not dependent upon intramembrane cleavage. In consequence, the moving junction continues to serve as a barrier for exclusion of MIC2, and as a result *rom4-ko* parasites accumulate uncleaved MIC2 as a distinct dot at the site where the PVM is sealed and is shed unprocessed.

To determine whether ROM4 is solely responsible for MPP1 activity, the fate of the MICs was examined quantitatively, both by microneme secretion assays and also via collection of culture supernatants during host cell invasion. MIC2 and MIC6 appeared to be exclusively processed by ROM4 whereas AMA1 showed residual shedding activity in the *rom4-ko* parasites. Intriguingly, the residual cleavage of AMA1 was not dependent upon stimulation of microneme secretion, and concordantly it could not be blocked by BAPTA-AM which chelate the mobilized intracellular calcium ions during this process (Carruthers *et al*., 1999). The presence of residual cleaved AMA1 was also confirmed in the *rom4-ko/rom5-ko* strain complemented with ROM5, as well as in *rom4-ko* transgenic parasites expressing a second FLAG-tagged copy of AMA1 by using different antibodies to exclude its presence on immunoblot as an artifact. These results imply that a minute amount of AMA1 is constitutively secreted and processed by a protease distinct from ROM4.

Because ROM5 was previously shown to cleave *P. falciparum* AMA1 in cell-based assays (Baker *et al*., 2006), it came as the most plausible candidate responsible for the residual shedding of AMA1 in *rom4-ko* parasites. A double knockout of *ROM4* and *ROM5* was generated and microneme secretion assays performed in this mutant clearly established that ROM5 is responsible for the residual cleavage of AMA1.

To determine if ROM5 cleaves other MICs that are normally expressed at very low level or for which no antibodies are available, we relied on the expression of SAG1-Ty-TM-CTD fusion constructs to facilitate detection of cleaved products. Interestingly, analysis of the SAG1-Ty-TM-CTD fusions revealed residual cleavage activity in *rom4-ko* parasites for AMA1, AMA2 and AMA4. Intriguingly, AMA2 and AMA4 were still processed in *rom4-ko/rom5-kd*, but this shedding was abrogated in *rom4-ko/rom5-ko*. This implies that minute amounts of ROM5 in the knockdown strains are able to cleave AMA2 and AMA4. Using this assay, we also show that ROM5 solely contributes to the cleavage of AMA1 and AMA2, and partially to AMA4 fusion constructs. Consistent with data reported for endogenous MIC2 and MIC6, the cleavage of corresponding SAG1-Ty-TM-CTD fusions was impaired in *rom4-ko* parasites. Intriguingly, abrogating microneme targeting of endogenous MIC2 substantially reduced its processing in *mic2-tailMut* parasites, while a residual processing was observed in *rom4-ko/rom5-ko/mic2-tailMut*. This indicated MIC2-tailMut is not processed by ROM5 but is presumably processed by another protease, presumably ROM2 that is also expressed in tachyzoites (Dowse *et al*., 2005; Shen *et al*., 2014b).

Phenotypically, the contribution of ROM5 to lytic cycle progression appeared very modest in the presence of ROM4, given that neither invasion, intracellular growth, egress nor gliding motility were impaired in *rom5-ko* parasites. In contrast, the deletion of *ROM5* in the *rom4-ko* strain led to an additional and significant drop in the invasion efficiency, which might be linked to the abrogation of residual cleavage of AMA1 but possibly also of other AMA members or yet uncharacterized substrates.

In summary, both ROM4 and ROM5 mediate transmembrane MICs cleavage and hence contributing to parasite invasion. ROM4 is responsible for the previously described constitutive and ubiquitous PM activity of MPP1, cleaving the majority of the MICs secreted via the micronemes (Opitz *et al*., 2002). By doing so ROM4 likely impacts on invasion by contributing to the correct apical orientation of the parasite. ROM5 has an ill-defined localization and appears to have limited access to the PM. In addition, ROM5 is only responsible for a small fraction of AMA1 cleavage indicative of function distinct from parasite reorientation. We also observed that ROM5 selectively cleaves AMA family members but not MIC2 or MIC6. Even when overexpressed in *rom4-ko/rom5-ko* strain, mycROM5 was only able to complement the absence of ROM5 but was unable to substitute for ROM4 function. The restricted access of ROM5 to a large pool of AMA1 is plausibly due to distinct lipid microenvironment or more likely as a result of compartmentalization, which would imply that a small pool of AMA1 traffics to a route independent of the micronemes and that ROM5 is not dispatched in significant amounts to the PM. Consistent with this model, the residual cleavage of AMA1 by ROM5 is insensitive to stimulation or blocking of microneme secretion, whereas MIC2 and MIC6 previously described as escorters traffic exclusively to the micronemes and upon secretion are cleaved by ROM4 instead. The biological significance of ROM5 and its contribution to invasion will require further investigation.

Experimental procedures

Ethics statement

This study was conducted according to the EU guidelines for the handling of laboratory animals.

Parasite culture

Derivatives of *T. gondii* RH *hxgprt*$^-$ strain parasites, as well as RH parasites lacking the *ku80* gene (*ku80*::diCre, Andenmatten *et al*., 2013) were maintained in confluent human foreskin fibroblast (HFF) monolayers with Dulbecco's modified Eagle's medium (DMEM; GIBCO, Invitrogen) supplemented with 5% foetal calf serum, 2 mM glutamine, and 25 mg ml^{-1} gentamicin.

© 2015 John Wiley & Sons Ltd, *Molecular Microbiology*

Cloning of DNA constructs

Table S2 contains a list of primers used in this study. To generate the plasmid pTub8-floxROM4-YFP-HXGPRT (pROM4^{flox}) for double-homologous recombination at the *ROM4* locus (ToxoDB accession no: TGME49_268590), 2 kb of the 5′-UTR and 3′-UTRs of the *ROM4* gene were amplified from genomic DNA purified from *ku80::diCre* parasites using listed primers. The *ROM4* 5′- and 3′UTRs were inserted into the plasmid p5RT70-floxKillerRed-YFP-HX (Andenmatten *et al*., 2013) between *Apa*I and *Sac*I sites, respectively, while the *mycROM4* coding sequence was subcloned between *EcoR*I/*Pac*I restriction sites in the plasmid pTub8-mycROM4-HXGPRT (Dowse *et al*., 2005). *TUB8* promoter was amplified from gDNA using listed primers and cloned upstream of mycROM4 in the modified plasmid above via *Stu*I restriction site.

To knockdown *ROM5* (ToxoDB accession no: TGME49_294690), we modified the plasmid pLIC-HA-FLAG-flox(3′UTR-SAG1-HXGPRT)-4xU1 (a gift from Dr. Markus Meissner) used for C-terminal knock-in and U1-mediated silencing (Pieperhoff *et al*., 2014). Genomic DNA corresponding to the *ROM5* C-terminus was amplified by listed primers and cloned into the plasmid pLIC-3ty-flox(3′UTR-SAG1-HXGPRT)-4xU1 between *Kpn*I and *Nsi*I sites. The resulting plasmid, pROM5-3ty-flox(3′UTR-SAG1-HXGPRT)-4xU1 (renamed pROM5-3ty-floxU1), was further modified to incorporate a *DHFR* selection cassette for use in the *rom4-ko* strain by removing the *DHFR* from p2854-DHFR via *Xba*I/*Nhe*I digestion and subcloning into pROM5-3ty-floxU1 via *Spe*I sites.

To generate the plasmid pSAG1-CAS9gfp-U6sgROM5 for guiding the CAS9 nuclease to exon 3 of *ROM5* to generate a double-strand-break (DSB), we used the Q5 mutagenesis kit from NEB (Cat# E0554S) according to the manufacturer's instructions. pSAG1-CAS9gfp-U6sgUPRT (a gift from Dr. David Sibley) (Shen and Sibley, 2014) was used as a template for the PCR reaction using the sgROM5 primer. The donor plasmid pROM5-Tub5CAT was used to repair the CAS9-generated DSB and was generated by genomic PCR amplification of 2 kb of *ROM5* 5′UTR from RHΔ*hxgprt*, and subsequent insertion between *Apa*I/*Cla*I sites in pTub5CAT (Soldati and Boothroyd, 1995).

The plasmid pTub8-mycROM5-DHFR was generated by subcloning via *Kpn*I/*Pac*I the Tub8mycROM5 fragment from pTub8mycROM5-HXGPRT plasmid (Dowse *et al*., 2005) into pMLC5-DHFR plasmid.

The plasmid pSK+A/AMA1WT-Flag (a gift from Dr. Gary Ward) described in (Parussini *et al*., 2012) was modified by insertion of a DHFR selection cassette from p2854-TgDHFR between XbaI/NheI sites and the resulting plasmid pSK+A/AMA1WT-Flag-DHFR was used to express an additional copy of AMA1 in *rom4-ko* strains.

Transfection, selection and isolation of Cre-excised parasites

Transfection of *T. gondii* was performed by electroporation (2,02 kV, 50 Ω, 25 μF) in an Electro Cell Manipulator 630 (BTX) with linearized plasmid DNA to generate stable lines, or with circular plasmid DNA for transient transfection.

To generate *rom4-ko* and *rom5-kd* strains, *ku80*::diCre were transfected with 60 μg of either *Afe*I/*Kpn*I-linearized pROM4^{flox}, or *BamH*I-linearized pROM5-3ty-floxU1 respectively. The parasite lines *rom4^{flox}*, as well as *rom5-3ty-floxU1* were isolated by selection with mycophenolic acid (MPA) (25 mg ml^{-1}) and supplementation with xanthine (50 mg ml^{-1}) as previously described (Donald *et al*., 1996), and clonal populations were generated upon limiting dilution cloning. To excise the floxed *mycROM4* at the *ROM4* locus, extracellular *rom4^{flox}* parasites were treated with 50 nM rapamycin for 4 h and passaged by limiting dilution cloning, upon which YFP-positive and *ROM4*-null clones were isolated.

To generate *rom5-kd* clones by U1-mediated gene silencing, *rom5-3ty-floxU1* were transiently transfected with 40 μg of pTub5Cre plasmid (Brecht *et al*., 1999), and immediately underwent limiting dilution cloning.

To generate the parasite line *rom4-ko*/*rom5-3ty-floxU1*, 60 μg of *BamHI*-linearized pROM5-3ty-flox-HXGPRT-DHFR-U1plasmid was used to transfect the *rom4-ko* parasite strain. Pyrimethamine-resistant *rom4-ko*/*rom5-3ty-floxU* was isolated after selection with 0.5 μM Pyrimethamine and was subsequently cloned by limiting dilution. Subsequently, the *rom4-ko*/*rom5-kd* was generated by transfecting pTub5Cre as outlined above.

To generate *rom4-ko/rom5-ko/mycROM5* parasites, pTub8-mycROM5-DHFR plasmid was linearized with *Pci*I and transfected into *rom4-ko/rom5-ko* strain.

CRISPR-CAS9-mediated disruption of ROM5 *and introduction of mutations in the* MIC2 *locus*

For generation of *rom5-ko* and *rom4-ko/rom5*-ko strains, we co-transfected pSAG1-CAS9gfp-U6gROM5 and *Apa*I-linearized pROM5-Tub5CAT plasmids into *rom5-3ty-floxU1* and *rom4-ko/rom5-3ty-floxU1* parasite lines respectively. The *rom5-ko* strain was obtained by limiting dilution cloning immediately following transfection. To isolate *rom4-ko/rom5-ko*, 30 h after transfection *rom4-ko/rom5-3ty-floxU1* were released from infected HFF monolayers with a 26G needle, purified and subjected to FACs analysis to isolate *rom4-ko* expressing CAS9-gfp and thereafter cloned into 96-well plates using Moflo-Astrios (Beckman Coulter). To distinguish GFP-signal among YFP parasites, GFP was excited with a 405-nm violet laser (Marcus and Raulet, 2013).

To facilitate homologous recombination at the *MIC2* locus and introduce microneme targeting motif mutations (^{721}SYHYY-RKRAR) in WT and *rom4-ko/rom5-ko* parasites, we co-transfected 30 μg of 100 bp double-stranded MIC2-mut oligonucleotides (dsOligo) with 15 μg pSAG1-CAS9gfp-U6gMIC2 to induce a DSB at the beginning of the coding sequence for the MIC2 cytoplasmic tail. GFP-positive cells were FACs sorted and cloned as described above. To generate N-terminal tagged *ROM5*, the above procedure was followed using primers listed in the supplementary table 2.

Semi-quantitative reverse transcriptase (RT) PCR

Total RNA was collected using Trizol reagent (GIBCO) and 1 μg was used to generate cDNA with Superscript II reverse transcriptase (Invitrogen) following the manufacturer's instruc-

© 2015 John Wiley & Sons Ltd, *Molecular Microbiology*

tions. Specific primers used for amplification of *TgROM5* and *Tubulin* cDNA by PCR are listed in supplementary table 2. All cDNA fragments were amplified using GoTaq in a 25-cycle PCR reaction.

Immunofluorescence assay (IFA)

Infected-HFF monolayers on coverslips were fixed with 4% paraformaldehyde (PFA) or 4% PFA/0.05% glutaraldehyde (Glu) for 10 min prior to quenching in 0.1M glycine/PBS. Cells were then permeabilized with 0.2% Triton X-100/PBS (PBS/Triton) and blocked in the same buffer supplemented with 2% BSA (PBS/Triton/BSA). Cells were incubated with primary antibodies (Abs) diluted in PBS/Triton/BSA for 60 min followed by PBS/Triton washes (3×5 min). Cells were incubated with secondary Abs (Alexa488- or Alexa594-conjugated goat anti-mouse or goat anti-rabbit IgGs) diluted at 1:3000 in PBS/Triton/BSA. Where appropriate, DAPI (4′,6-diamidino-2-phenylindole) staining of parasite and HFF nuclei was performed by incubating cells in DAPI (50 μg ml^{-1} in PBS) prior to washing as outlined previously. Coverslips were mounted in Fluoromount G (Southern Biotech) on glass slides and stored at 4°C in the dark. Images were collected using an LSM 700 confocal scanning microscope (Zeiss).

For analysis of MICs during invasion, freshly released parasites (5×10^6) were added to confluent HFF monolayer-coated coverslips and placed on ice for 20 min. Invasion was allowed to take place during 2 min at 38.5°C and subsequently blocked by fixation in 4% PFA for 30 min. Following washes, cells were permeabilized with 0.1% saponin for 10 min and blocked for 30 min with 10% fetal bovine serum. IFAs were performed as described previously (El Hajj *et al*., 2008).

Western blotting

Western blotting analyses were performed as previously described (Sheiner *et al*., 2010).

Red/green invasion assay

The red/green invasion assay was used to distinguish non-invaded from invaded parasites and is described here briefly. Freshly egressed parasites were inoculated on 24-well plates containing coverslips seeded with HFF monolayers and were allowed to settle for 15 min at 4°C. Invasion was allowed to take place for 30 min at 37°C prior to fixation using PFA/Glu. Standard non-permeabilizing IFA was performed by staining extracellular parasites with monoclonal anti-SAG1 Abs, followed by permeabilization with PBS/Triton and subsequent staining of invaded parasites with polyclonal anti-GAP45 Abs. Respective secondary antibodies were used as described previously. For each experiment, at least 50 parasites were counted, each time distinguishing non-invaded (red) from invaded (green) parasites. Three independent biological replicates were completed.

Attachment assay

Attachment of *T. gondii* parasites to HFF monolayers was assessed as previously described (Mueller *et al*., 2013). Briefly, freshly egressed parasites were incubated in Endobuffer (Endo *et al*., 1987) containing 1 μM Cytochalasin D for 15 min at 37°C. Endobuffer was replaced by DMEM containing 1 μM Cytochalasin D and incubated for 15 min at 37°C prior to fixation with PFA/Glu. Standard, non-permeabilizing IFA was performed by staining parasites with monoclonal anti-SAG1 Abs and the number of attached parasites per field was counted.

Induced egress assay

Freshly egressed parasites were added to HFF monolayer layers and grown for ~ 30 h at 37°C. For IFA-based analysis of parasite egress, infected HFF monolayers were incubated for 7 min at 37°C with serum-free DMEM containing either 3 μM of the Ca^{2+} ionophore A23187 (from *Streptomyces chartreusensis*, Calbiochem) to induce egress, or DMSO as a control. Cells were fixed with PFA/Glu, and IFA was performed using anti-GAP45 Abs. One hundred vacuoles were counted per strain in three independent experiments, and the number of lysed vacuoles was scored.

For analysis of egress by live video microscopy, parasites were grown for ~ 30 h at 37°C on 5 mm Fluorodishes (World Precision Instruments) seeded with HFF monolayers. To induce egress, A23187 (3 μM) was added to infected-HFF monolayers and live image sequences (2 images per second) were taken with the Zeiss Axiovert 200M wide-field fluorescent microscope. Movies were processed using NIS-Elements software.

Gliding motility assay

Freshly egressed parasites were pelleted, resuspended in calcium-saline solution and added to FBS-coated coverslips (50% in PBS) prior to incubation for 30 min at 37°C and fixation with PFA/Glu. Trails deposited on the coverslips were visualized following standard non-permeabilizing IFA using anti-SAG1 Abs. Trail length was measured using ImageJ software and presented according to parasite body lengths as previously described (Barragan and Sibley, 2002).

For live imaging of motility patterns, freshly egressed parasites were resuspended in calcium-saline solution and allowed to settle on FBS-coated 5 mm Fluorodishes (World Precision Instruments) for 5 min. Time-lapse images were obtained upon addition of calcium-saline solution containing A23187 1 μM, and time-lapse images were recorded every second for a total of 5 min. Movies were processed using NIS-Elements software and the characteristic motility patterns were quantified according to established criteria (Hakansson *et al*., 1999).

Plaque, intracellular growth and competition assays

For plaque assays, 100 parasites were inoculated onto 6-well plates seeded with HFF monolayers, prior to growth for 8 days at 37°C. Plaques were visualized by fixing with 4% PFA/Glu and staining with Crystal Violet (0.1%).

For intracellular growth assays, HFF monolayers were inoculated with freshly egressed parasites and after 1 h the HFF monolayer was washed (×3) with DMEM to remove

© 2015 John Wiley & Sons Ltd, *Molecular Microbiology*

uninvaded parasites. Invaded parasites were allowed to grow for 30 h at 37°C prior to fixation with 4% PFA and subsequent IFA using anti-GAP45 Abs. The number of parasites per vacuole was counted from a total of 100 vacuoles in three independent experiments.

Competition growth assays of *rom4-ko/rom5-3ty-floxU1 vs. rom4-ko/rom5-ko* were performed by mixing equal numbers of the two strains and subsequent inoculation onto HFF monolayers in 24 well plates with and without coverslips. Parasites were allowed to invade for 1 h before washing and incubation for 24 h at 37°C. Upon egress, parasites were repeatedly inoculated onto 24-well coverslips seeded with HFF monolayers.

Secretion assays

Microneme secretion assays were performed as described previously but with minor modifications (Opitz *et al*., 2002). Briefly, freshly egressed parasites were washed twice using intracellular buffer (IC; 5 mM NaCl, 142 mM KCl, 2 mM EGTA, 1 mM MgCl2, 5.6 mM glucose, 25 mM HEPES-KOH, pH 7.2), before secretion was induced by addition of 2% (v/v) ethanol in serum-free DMEM at 37°C for 20 min. Excreted secreted antigens (ESA) were collected upon sequential centrifugation; following an initial centrifugation for 5 min/4°C/1000 g, supernatant was transferred to a new tube and spun again at higher speed (5 min/4°C/2000 g) to remove any final traces of pellet. The final supernatant was collected and analyzed by immunoblotting with specific Abs.

To analyze transmembrane MICs on the parasite surface by IFA, freshly egressed parasites were washed with IC buffer prior to induction of microneme secretion for 5 min as described above. Parasites were settled on gelatin-coated (0.1% in PBS) coverslips in 24-well plates and centrifuged for 1 min/4°C/500 g. Fixed parasites were then processed by IFA as described above.

For analysis of shed MICs during invasion, freshly egressed parasites were incubated on HFF monolayers in DMEM without serum and allowed to invade for 60 min at 37°C. The culture supernatant was collected and concentrated 20 × with Centricon® centrifugal filter units (Millipore) and analyzed by western blotting using specific Abs.

For analysis of secreted SAG1-Ty-TM-CTD fragments by western blot, HFF monolayers infected for ~ 30 h with parasites individually transiently transfected with different SAG1-Ty-TM-CTD chimeras were scraped from 6 cm diameter dishes in the presence of IC buffer. Where stated, parasites were transiently co-transfected with pTub8mycGFP as an internal loading control. The resulting suspension was centrifuged for 5 min/4°C/1000 g and the pellet was collected and processed for western blot as described previously (Opitz *et al*., 2002).

Antibodies used in this study

The following antibodies were used in this study: T34A11 mAb anti-MIC2 (Achbarou *et al*., 1991), rabbit anti-AMA1 (Lamarque *et al*., 2014), polyclonal anti-ROM4 (Sheiner *et al*., 2008), anti-Flag mAb (Sigma), rabbit anti-GAP45, rabbit anti-Myc, mAb anti-Myc supernatant, mAb anti-Ty1 supernatant, mAb anti-GRA1 (Sibley *et al*., 1995), rabbit anti-MIC6 (Reiss *et al*., 2001), rabbit anti-MIC4 (Reiss *et al*., 2001), and mAb T52A3 anti-ROP1 (unpublished).

Acknowledgements

We are very grateful to Dr. Markus Meissner for the *ku80::diCre* strain and plasmids for GOI excision and Dr. David Sibley for the pSAG1-CAS9gfp-U6sgUPRT plasmid. We thank Dr. Michael J. Blackman and Dr. Chetan Chitnis for useful discussions; Dr. Hayley Bullen for critical reading of the manuscript and Dr. Jean-Pierre Aubry-Lachainaye for assistance at the FACS facility. M.L and A.G received funding from Laboratoire d'Excellence (LabEx) (ParaFrap ANR-11-LABX-0024). G.R. received funding from the EVIMalaR PhD Fellowship through the EU FP7/2007–2013 grant n°242095. J-B.M is supported by the Swiss National Foundation (FN3100A0-116722). D. S-F is an International Scholar of the Howard Hughes Medical Institute.

Conflict of interests

The authors declare no conflict of interest.

References

Achbarou, A., Mercereau-Puijalon, O., Autheman, J.M., Fortier, B., Camus, D., and Dubremetz, J.F. (1991) Characterization of microneme proteins of *Toxoplasma gondii*. *Mol Biochem Parasitol* **47:** 223–233.

Andenmatten, N., Egarter, S., Jackson, A.J., Jullien, N., Herman, J.P., and Meissner, M. (2013) Conditional genome engineering in *Toxoplasma gondii* uncovers alternative invasion mechanisms. *Nat Methods* **10:** 125–127.

Baker, R.P., Wijetilaka, R., and Urban, S. (2006) Two *Plasmodium rhomboid* proteases preferentially cleave different adhesins implicated in all invasive stages of malaria. *PLoS Pathog* **2:** e113.

Bargieri, D.Y., Andenmatten, N., Lagal, V., Thiberge, S., Whitelaw, J.A., Tardieux, I., *et al*. (2013) Apical membrane antigen 1 mediates apicomplexan parasite attachment but is dispensable for host cell invasion. *Nat Commun* **4:** 2552.

Barragan, A., and Sibley, L.D. (2002) Transepithelial migration of *Toxoplasma gondii* is linked to parasite motility and virulence. *J Exp Med* **195:** 1625–1633.

Brecht, S., Erdhart, H., Soete, M., and Soldati, D. (1999) Genome engineering of *Toxoplasma gondii* using the site-specific recombinase Cre. *Gene* **234:** 239–247.

Brecht, S., V., Carruthers, B., Ferguson, D.J., Giddings, O.K., Wang, G., Jakle, U., *et al*. (2001) The toxoplasma micronemal protein MIC4 is an adhesin composed of six conserved apple domains. *J Biol Chem* **276:** 4119–4127.

Brossier, F., Jewett, T.J., Lovett, J.L., and Sibley, L.D. (2003) C-terminal processing of the toxoplasma protein MIC2 is essential for invasion into host cells. *J Biol Chem* **278:** 6229–6234.

Brossier, F., Jewett, T.J., Sibley, L.D., and Urban, S. (2005) A spatially localized rhomboid protease cleaves cell surface adhesins essential for invasion by *Toxoplasma*. *Proc Natl Acad Sci USA* **102:** 4146–4151.

© 2015 John Wiley & Sons Ltd, *Molecular Microbiology*

Brydges, S.D., X., Zhou, W., Huynh, M.H., Harper, J.M., Mital, J., Adjogble, K.D., *et al*. (2006) Targeted deletion of MIC5 enhances trimming proteolysis of *Toxoplasma* invasion proteins. *Eukaryot Cell* **5:** 2174–2183.

Buguliskis, J.S., Brossier, F., Shuman, J., and Sibley, L.D. (2010) Rhomboid 4 (ROM4) affects the processing of surface adhesins and facilitates host cell invasion by *Toxoplasma gondii*. *PLoS Pathog* **6:** e1000858.

Carruthers, V.B., and Sibley, L.D. (1997) Sequential protein secretion from three distinct organelles of *Toxoplasma gondii* accompanies invasion of human fibroblasts. *Eur J Cell Biol* **73:** 114–123.

Carruthers, V.B., Giddings, O.K., and Sibley, L.D. (1999) Secretion of micronemal proteins is associated with toxoplasma invasion of host cells. *Cell Microbiol* **1:** 225–235.

Carruthers, V.B., Sherman, G.D., and Sibley, L.D. (2000) The Toxoplasma adhesive protein MIC2 is proteolytically processed at multiple sites by two parasite-derived proteases. *J Biol Chem* **275:** 14346–14353.

Cerede, O., Dubremetz, J.F., Soete, M., Deslee, D., Vial, H., Bout, D., and Lebrun, M. (2005) Synergistic role of micronemal proteins in *Toxoplasma gondii* virulence. *J Exp Med* **201:** 453–463.

Di Cristina, M., Spaccapelo, R., Soldati, D., Bistoni, F., and Crisanti, A. (2000) Two conserved amino acid motifs mediate protein targeting to the micronemes of the apicomplexan parasite *Toxoplasma gondii*. *Mol Cell Biol* **20:** 7332–7341.

Dobrowolski, J.M., and Sibley, L.D. (1996) *Toxoplasma* invasion of mammalian cells is powered by the actin cytoskeleton of the parasite. *Cell* **84:** 933–939.

Donahue, C.G., V., Carruthers, B., Gilk, S.D., and Ward, G.E. (2000) The *Toxoplasma* homolog of *Plasmodium* apical membrane antigen-1 (AMA-1) is a microneme protein secreted in response to elevated intracellular calcium levels. *Mol Biochem Parasitol* **111:** 15–30.

Donald, R.G., Carter, D., Ullman, B., and Roos, D.S. (1996) Insertional tagging, cloning, and expression of the *Toxoplasma gondii* hypoxanthine-xanthine-guanine phosphoribosyltransferase gene. Use as a selectable marker for stable transformation. *J Biol Chem* **271:** 14010–14019.

Dowse, T., and Soldati, D. (2004) Host cell invasion by the apicomplexans: the significance of microneme protein proteolysis. *Curr Opin Microbiol* **7:** 388–396.

Dowse, T.J., Pascall, J.C., Brown, K.D., and Soldati, D. (2005) Apicomplexan rhomboids have a potential role in microneme protein cleavage during host cell invasion. *Int J Parasitol* **35:** 747–756.

El Hajj, H., Papoin, J., Cerede, O., Garcia-Reguet, N., Soete, M., Dubremetz, J.F., and Lebrun, M. (2008) Molecular signals in the trafficking of *Toxoplasma gondii* protein MIC3 to the micronemes. *Eukaryot Cell* **7:** 1019–1028.

Endo, T., Tokuda, H., Yagita, K., and Koyama, T. (1987) Effects of extracellular potassium on acid release and motility initiation in *Toxoplasma gondii*. *J Protozool* **34:** 291–295.

Fortes, P., Cuevas, Y., Guan, F., Liu, P., Pentlicky, S., Jung, S.P., *et al*. (2003) Inhibiting expression of specific genes in mammalian cells with 5′ end-mutated U1 small nuclear RNAs targeted to terminal exons of pre-mRNA. *Proc Natl Acad Sci USA* **100:** 8264–8269.

Frixione, E., Mondragon, R., and Meza, I. (1996) Kinematic analysis of *Toxoplasma gondii* motility. *Cell Motil Cytoskeleton* **34:** 152–163.

Garcia-Reguet, N., Lebrun, M., Fourmaux, M.N., Mercereau-Puijalon, O., Mann, T., Beckers, C.J., *et al*. (2000) The microneme protein MIC3 of *Toxoplasma gondii* is a secretory adhesin that binds to both the surface of the host cells and the surface of the parasite. *Cell Microbiol* **2:** 353–364.

Gunderson, S.I., Polycarpou-Schwarz, M., and Mattaj, I.W. (1998) U1 snRNP inhibits pre-mRNA polyadenylation through a direct interaction between U1 70K and poly(A) polymerase. *Mol Cell* **1:** 255–264.

Hakansson, S., Morisaki, H., Heuser, J., and Sibley, L.D. (1999) Time-lapse video microscopy of gliding motility in *Toxoplasma gondii* reveals a novel, biphasic mechanism of cell locomotion. *Mol Biol Cell* **10:** 3539–3547.

Howell, S.A., Hackett, F., Jongco, A.M., Withers-Martinez, C., Kim, K., Carruthers, V.B., and Blackman, M.J. (2005) Distinct mechanisms govern proteolytic shedding of a key invasion protein in apicomplexan pathogens. *Mol Microbiol* **57:** 1342–1356.

Hu, K., Mann, T., Striepen, B., Beckers, C.J., Roos, D.S., and Murray, J.M. (2002) Daughter cell assembly in the protozoan parasite Toxoplasma gondii. *Mol Biol Cell* **13:** 593–606.

Huynh, M.H., and Carruthers, V.B. (2006) Toxoplasma MIC2 is a major determinant of invasion and virulence. *PLoS Pathog* **2:** e84.

Huynh, M.H., Rabenau, K.E., Harper, J.M., Beatty, W.L., Sibley, L.D., and Carruthers, V.B. (2003) Rapid invasion of host cells by *Toxoplasma* requires secretion of the MIC2-M2AP adhesive protein complex. *EMBO J* **22:** 2082–2090.

Jewett, T.J., and Sibley, L.D. (2003) Aldolase forms a bridge between cell surface adhesins and the actin cytoskeleton in apicomplexan parasites. *Mol Cell* **11:** 885–894.

Kessler, H., Herm-Gotz, A., Hegge, S., Rauch, M., Soldati-Favre, D., Frischknecht, F., and Meissner, M. (2008) Microneme protein 8 – a new essential invasion factor in *Toxoplasma gondii*. *J Cell Sci* **121:** 947–956.

Lagal, V., Binder, E.M., Huynh, M.H., Kafsack, B.F., Harris, P.K., Diez, R., *et al*. (2010) Toxoplasma gondii protease TgSUB1 is required for cell surface processing of micronemal adhesive complexes and efficient adhesion of tachyzoites. *Cell Microbiol* **12:** 1792–1808.

Lamarque, M.H., Roques, M., Kong-Hap, M., Tonkin, M.L., Rugarabamu, G., Marq, J.B., *et al*. (2014) Plasticity and redundancy among AMA-RON pairs ensure host cell entry of *Toxoplasma* parasites. *Nat Commun* **5:** 4098.

Lebrun, M., Michelin, A., El Hajj, H., Poncet, J., Bradley, P.J., Vial, H., and Dubremetz, J.F. (2005) The rhoptry neck protein RON4 re-localizes at the moving junction during *Toxoplasma gondii* invasion. *Cell Microbiol* **7:** 1823–1833.

Marcus, A., and Raulet, D.H. (2013) A simple and effective method for differentiating GFP and YFP by flow cytometry using the violet laser. *Cytometry A* **83:** 973–974.

Meissner, M., Reiss, M., Viebig, N., Carruthers, V.B., Toursel, C., Tomavo, S., *et al*. (2002) A family of transmembrane microneme proteins of *Toxoplasma gondii* contain EGF-like domains and function as escorters. *J Cell Sci* **115:** 563–574.

Mital, J., Meissner, M., Soldati, D., and Ward, G.E. (2005)

© 2015 John Wiley & Sons Ltd, *Molecular Microbiology*

Conditional expression of *Toxoplasma gondii* apical membrane antigen-1 (TgAMA1) demonstrates that TgAMA1 plays a critical role in host cell invasion. *Mol Biol Cell* **16:** 4341–4349.

Mueller, C., Klages, N., Jacot, D., Santos, J.M., Cabrera, A., Gilberger, T.W., *et al*. (2013) The Toxoplasma protein ARO mediates the apical positioning of rhoptry organelles, a prerequisite for host cell invasion. *Cell Host Microbe* **13:** 289–301.

Opitz, C., Di Cristina, M., Reiss, M., Ruppert, T., Crisanti, A., and Soldati, D. (2002) Intramembrane cleavage of microneme proteins at the surface of the apicomplexan parasite *Toxoplasma gondii*. *EMBO J* **21:** 1577–1585.

Parussini, F., Tang, Q., Moin, S.M., Mital, J., Urban, S., and Ward, G.E. (2012) Intramembrane proteolysis of *Toxoplasma* apical membrane antigen 1 facilitates host-cell invasion but is dispensable for replication. *Proc Natl Acad Sci USA* **109:** 7463–7468.

Pieperhoff, M.S., Pall, G.S., Jimenez-Ruis, E., Das, S., Wong, E.H., Heng, J., *et al*. (2014) Conditional U1 Gene Silencing in *Toxoplasma gondii* bioRxiv. doi:10.1101/008649.

Poukchanski, A., Fritz, H.M., Tonkin, M.L., Treeck, M., Boulanger, M.J., and Boothroyd, J.C. (2013) *Toxoplasma gondii* sporozoites invade host cells using two novel paralogues of RON2 and AMA1. *PLoS ONE* **8:** e70637.

Reiss, M., Viebig, N., Brecht, S., Fourmaux, M.N., Soete, M., Di Cristina, M., *et al*. (2001) Identification and characterization of an escorter for two secretory adhesins in *Toxoplasma gondii*. *J Cell Biol* **152:** 563–578.

Santos, J.M., Ferguson, D.J., Blackman, M.J., and Soldati-Favre, D. (2011) Intramembrane cleavage of AMA1 triggers *Toxoplasma* to switch from an invasive to a replicative mode. *Science* **331:** 473–477.

Sheiner, L., Dowse, T.J., and Soldati-Favre, D. (2008) Identification of trafficking determinants for polytopic rhomboid proteases in Toxoplasma gondii. *Traffic* **9:** 665–677.

Sheiner, L., Santos, J.M., Klages, N., Parussini, F., Jemmely, N., Friedrich, N., Ward, G.E., and Soldati-Favre, D. (2010) Toxoplasma gondii transmembrane microneme proteins and their modular design. *Mol Microbiol* **77:** 912–929.

Shen, B., and Sibley, L.D. (2014) Toxoplasma aldolase is required for metabolism but dispensable for host-cell invasion. *Proc Natl Acad Sci USA* **111:** 3567–3572.

Shen, B., Brown, K.M., Lee, T.D., and Sibley, L.D. (2014a) Efficient gene disruption in diverse strains of *Toxoplasma gondii* using CRISPR/CAS9. *MBio* **5:** e01114.

Shen, B., Buguliskis, J.S., Lee, T.D., and Sibley, L.D. (2014b) Functional analysis of rhomboid proteases during Toxoplasma invasion. *MBio* **5:** e01795-14.

Sibley, L.D. (2010) How apicomplexan parasites move in and out of cells. *Curr Opin Biotechnol* **21:** 592–598.

Sibley, L.D. (2013) The roles of intramembrane proteases in protozoan parasites. *Biochim Biophys Acta* **1828:** 2908–2915.

Sibley, L.D., I., Niesman, R., Parmley, S.F., and Cesbron-Delauw, M.F. (1995) Regulated secretion of multi-lamellar vesicles leads to formation of a tubulo-vesicular network in host-cell vacuoles occupied by *Toxoplasma gondii*. *J Cell Sci* **108** (Part 4): 1669–1677.

Sidik, S.M., Hackett, C.G., Tran, F., Westwood, N.J., and Lourido, S. (2014) Efficient genome engineering of *Toxoplasma gondii* using CRISPR/Cas9. *PLoS ONE* **9:** e100450.

Soldati, D., and Boothroyd, J.C. (1995) A selector of transcription initiation in the protozoan parasite *Toxoplasma gondii*. *Mol Cell Biol* **15:** 87–93.

Zhou, X.W., Blackman, M.J., Howell, S.A., and Carruthers, V.B. (2004) Proteomic analysis of cleavage events reveals a dynamic two-step mechanism for proteolysis of a key parasite adhesive complex. *Mol Cell Proteomics* **3:** 565–576.

Supporting information

Additional supporting information may be found in the online version of this article at the publisher's web-site.

© 2015 John Wiley & Sons Ltd, *Molecular Microbiology*